Role of hydrometeorological variables and catchment area to flood generation over the monsoonal climate region of India

Authors

Saran Aadhar[1,2], Efrat Morin[3], Utkarsh Gupta[1]

Affiliations

1. Civil and Infrastructure Engineering, Indian Institute of Technology (IIT) Jodhpur, Jodhpur, India
2. ~~Center for Emerging Technologies for Sustainable Development (CETSD),~~Environmental and Sustainability Engineering, IIT Jodhpur, Jodhpur, India
3. The Fredy & Nadine Herrmann Institute of Earth Sciences, Hebrew University of Jerusalem, Jerusalem, Israel

Corresponding Author: Saran Aadhar (saran.aadhar@iitj.ac.in)

Abstract:

Indian River basins experience frequent flooding during the Indian summer monsoon ~~rainfall~~ and pose several challenges ~~to~~for the region's large population ~~of the region. To effectively manage flood risk in the region, a better understanding of flood generating mechanisms is essential~~, yet the hydrometeorological and catchment-scale drivers ~~controlling~~that control flood processes ~~are~~remain poorly explored across India. To effectively manage flood risk in the densely populated Indian region, it is essential to

understand how the temporal properties of precipitation and runoff generate floods across different aridity regimes within a large catchment, and which specific areas of a large, climatically heterogeneous basin generate the runoff that drives downstream flood peaks. In this study, we address these gaps and examine the role of hydrometeorological variables (such as precipitation and surface runoff) and catchment area in the flood occurrence in the Godavari River basin (one of the largest river basins ~~(Godavari River basin) of~~in the Indian Subcontinent) using observed and VIC-simulated datasets. Based on the temporal analysis of precipitation, runoff, and streamflow, we show that ~~floods caused by multiple high-intensity precipitation days predominantly occur in the semi-humid sub-basins (Tekra, Pathagudam, Perur, and Polavaram) of the Godavari River. The~~the majority of floods in the semi-humid sub-basins ~~are~~(Tekra, Pathagudam, Perur, and Polavaram) are predominantly associated with 10 to 11 days of accumulated precipitation, having multiple high-intensity precipitation events prior to flood. In contrast, the ~~majority of~~ floods in the semi-arid region of Godavari (Mancherial sub-basin) are triggered by a single high-intensity precipitation day and are associated with short-duration (2 days) accumulated precipitation. In addition to temporal analysis, we ~~also~~ performed Empirical Orthogonal ~~Functions~~Function (EOF) analysis using precipitation, runoff, and streamflow data to identify the specific sub-regions that disproportionately generate flood-causing runoff (flood-dominant catchment ~~area.~~areas). Our results demonstrate that central and downstream areas of the basin contribute ~~disproportionately~~ dominantly to flood occurrence, ~~with the Tekra sub-basin~~ generating substantially higher runoff ~~due to favorable catchment characteristics.~~in the Tekra sub-basin. Overall, this study moves beyond basin-averaged flood attribution and advances

understanding of flood-generating mechanisms over the Godavari River basin, which can be helpful for ~~flood control and~~duration-informed forecasting and catchment-scale flood management during the monsoonal climate of the Indian Subcontinent.

Keywords: Flood mechanisms, Hydrometeorology, Catchment Characteristics, Godavari basin, Monsoonal climate.

Formatted: Left

Highlights

- **The majority of floods in the semi-humid regions of the Godavari River predominantly occur due to multiple high-intensity rainfall days**
- **Floods in the semi-arid Mancherial sub-basin are triggered by a single high-intensity precipitation event**
- **Central and downstream areas of the Godavari River basin dominate in the flood occurrence**
- **High runoff generation in the Tekra sub-basin plays an important role in downstream flooding in the Godavari River basin**

1. Introduction

Floods are ~~one of~~among the costliest natural disasters, ~~which cause~~causing severe damage to infrastructure and socio-economic conditions. According to the World Bank report in 2006, floods caused damage of 163 million US$ annually during the 1999–2005 period in India. Moreover, ~~the occurrence of floods has~~flood occurrences have increased in India ~~in~~over the last few decades under ~~the~~a warming climate, ~~which has affected~~affecting millions of people in the region (Ali et al., 2019; Gosain et al., 2006;

Gupta and Nair, 2011; Milly et al., 2002). For instance, ~~recently occurred~~recent flood events in the Indian sub-continent (i.e., 2018 Kerala flood, 2014 Jammu and Kashmir flood, and 2013 Uttarakhand flood) caused enormous ~~loss~~losses of property and human lives (Lindell et al., 2019; Mishra et al., 2018; Ray et al., 2019). Due to global warming, the frequency of high-intensity precipitation events has increased at the regional and global scales ~~(Allan and Soden, 2007; Gosain et al., 2006; Guerreiro et al., 2018; Min et al., 2011; Rogger et al., 2017; Trenberth et al., 2003; Ummenhofer et al., 2011)~~(Allan and Soden, 2007; Gosain et al., 2006; Guerreiro et al., 2018; Min et al., 2011; Nanditha and Mishra, 2024; Rogger et al., 2017; Trenberth et al., 2003; Ummenhofer et al., 2011), which instigated the increase in flood magnitude and frequency across the globe (Ali et al., 2019; Gosain et al., 2006; Gupta and Nair, 2011; Kundzewicz et al., 2014; Milly et al., 2002). Therefore, an improved understanding of flood processes is required in the densely populated Indian sub-continent to reduce the severe impact of flood events.

Flood mechanisms comprise multiple processes that control the intensity and magnitude of ~~flow in a~~ river flow. In the monsoonal climate, the majority of floods occur primarily due to high-intensity precipitation events (Ali et al., 2019; Garg and Mishra, 2019; Nanditha et al., 2022; Nanditha and Mishra, 2022). However, static factors of catchment properties (basin slope, geometry, land use and land cover, drainage density, drainage area, and soil parameters) can also have an essential role in the flood generation mechanism, apart from extreme precipitation (Blöschl et al., 2017, 2013; Merz and Blöschl, 2003; Tarasova et al., 2019). For example, forest land cover generates less runoff than arable land cover during storm events (Lane, 2017; Marc and Robinson,

2007). Recent study (Sharma and Mujumdar, 2024) found that baseflow contributes significantly to the flood occurrence in Peninsular India.

To examine flood control processes, several causative processes and storylines (e.g., high precipitation, rain on snow, cloudburst, excess runoff) have been used in previous studies ~~(Berghuijs et al., 2016; Keller et al., 2018; Li et al., 2019; Nied et al., 2014; Tarasova et al., 2019; Viglione et al., 2010)~~(Berghuijs et al., 2016; Keller et al., 2018; Li et al., 2019; Nanditha and Mishra, 2022; Nied et al., 2014; Sharma and Mujumdar, 2024; Tarasova et al., 2019; Viglione et al., 2010). These causative processes include the hydroclimatic, hydrological, and hydrograph perspectives to better understand the flooding mechanisms (Tarasova et al., 2019). Based on the causative classification, ~~the~~ flood mechanisms, considering ~~the~~ weather systems, storm patterns, moisture transport, and weather circulation, are classified in the hydroclimatic perspective (Blöschl et al., 2013; Grams et al., 2014). ~~Hydrograph~~The hydrograph perspective uses discharge time-series data to evaluate ~~the different~~ hydrographs~~, which~~ that show distinct flood~~-~~ generation mechanisms (Tarasova et al., 2019). Under the hydrological perspective, hydrometeorological variables within the catchment, soil moisture information, and hydrological processes (i.e., saturation excess and infiltration) are considered (Berghuijs et al., 2016; Nied et al., 2014; Sikorska et al., 2015).

In some cases, multiple criteria were used in the evaluation of flood processes, for example, short-duration heavy rainfall and long-duration rainfall (with and without high-intensity rainfall) (Keller et al., 2018; Li et al., 2019; Nied et al., 2014; Tarasova et al., 2019). Additionally, the spatial variability of hydrometeorological variables within the catchment is also crucial to the flooding mechanism. For instance, Freyberg et al. (2014)

found that a small portion of the catchment induces large streamflow in a pre-alpine catchment during ~~the~~ rainy days, ~~which causes~~causing floods in the basin. Therefore, determining the flood-dominating catchment areas based on ~~the~~ hydrometeorological and catchment properties ~~before~~prior to the peak flood is crucial for understanding flood processes. Overall, we need to thoroughly ~~analyze~~analyse the temporal and spatial properties of hydrometeorological variables ~~for a~~to better ~~understanding of~~understand flood generation mechanisms.

Flood mechanisms remain largely unexplored in large rivers within the monsoonal climate of India, which presents unique ~~conditions of hydrometeorology~~hydrometeorological and catchment ~~properties~~conditions. For instance, large river basins ~~of~~in India have dry soil conditions in the pre-monsoon season~~, while~~ and extremely wet soil conditions during the mid- and late monsoon. Moreover, large basins exhibit a variety of climate zones, ~~topographies~~topography, soil parameters, and vegetation ~~covers, which result~~cover, resulting in different hydrological responses during the monsoon season. Therefore, the goal of the present study is to understand the major flood-generating mechanisms ~~in~~across different aridity regimes within one of the largest river basins in the Indian Subcontinent, the Godavari River basin. Using the Variable Infiltration Capacity [VIC; (Cherkauer et al., 2003; Liang et al., 1996, 1994)] simulated hydrological variables and observed meteorological datasets, first, we examine the temporal variability of hydrometeorological variables (precipitation and surface runoff) before the peak streamflow events to identify the dominating flood processes. Later, we evaluate the spatial variability of hydrometeorological variables to identify flood-

dominant catchment areas~~, which are~~ associated with ~~the occurrence of~~ downstream flood events.

2. Study area

The Godavari River basin (Figure 1) is the second largest river basin in India, after the Ganges basin. The Godavari River witnessed many severe floods in the past decades (Garg and Mishra, 2019; Mujumdar et al., 1969; Rakhecha and Singh, 2017; Rakhecha, 2002), which affected the livelihood and life of millions of people in the basin. For instance, the floods during the ~~year~~years 1969 and 1976 in the Indravati (tributary of the Godavari River) stream posed severe damage in the basin (Garg and Mishra, 2019; Mujumdar et al., 1969; Rakhecha, 2002), which resulted in enormous loss of property and human lives. Similarly, the year 1986 flood in the downstream part of the river affected millions of people, with a loss of more than 250 lives (Rakhecha and Singh, 2017; The Hindu, 2011). Moreover, the high flow level in the Godavari River during 2019 displaced more than 17000 people of Andhra Pradesh (https://floodlist.com/asia/india-godavari-river-flood-andhra-pradesh-august-2019).

The Godavari river basin has a drainage area of approximately 312,800 km^2 and a river length of 1,465 km. The basin covers six Indian states (Maharashtra, Karnataka, Andhra Pradesh, Telangana, Chhattisgarh, and Odisha) and is located in peninsular India. Godavari River originates from Triambakeshwar, a high-altitude (1067 m above sea level, masl) place in the Nasik district of Maharashtra. The river flows eastward from the Western Ghats to the Bay of Bengal across the Deccan Plateau (Figure 1). The basin exhibits significant elevation variability (Figure 1a), ranging from a flat plain (below 10 masl) to a hill range (above 1200 masl). Due to its low elevation, the downstream part of

the basin has experienced numerous floods in the past. For instance, the irrigation department of Andhra Pradesh issued 22 flood warnings ~~between 1962 and 1990~~ at Dowlaiswarm (~~the~~a place ~~is located~~ near the river mouth) between 1962 and 1990 (Nageswara Rao, 2001). The basin also shows a large diversification in land use and land cover (LULC). The upper part of the basin is primarily covered by irrigated agricultural land, ~~while~~whereas the downstream region ~~has~~is covered by forest land ~~cover~~ (Figure 1b).

There is a large spatial variation in climate conditions across the basin. The annual mean temperature of the basin ~~varies between~~ranges from 20 to 30 °C~~,~~ and is primarily correlated with elevation (Figure 1c). ~~Moreover, the~~The Godavari river basin receives ~~the majority of~~most precipitation ~~in the form of~~as rainfall (~~without any~~no snowfall), which occurs predominantly ~~occurs~~ during the monsoon season (June to September), with large spatial variability in the annual mean (Figure 1d). The annual mean precipitation varies from 500 to 1200 mm, where the eastern part of the basin receives a large amount of rainfall, while the western part receives less than 600 mm of precipitation during the monsoon season (Figure 1d). Based on the Aridity Index (AI; the ratio of mean annual precipitation and mean annual potential evapotranspiration), the western part of the Godavari basin falls under the semi-arid region ($0.2 \leq AI < 0.5$) due to less rainfall (Figure S1), while the central and eastern parts of the basin fall under dry semi-humid and wet semi-humid ~~region~~regions, respectively (Figure S1). Detailed information ~~about the~~on basin elevation, land use and land cover (LULC), precipitation, and temperature can be ~~obtained from~~found in Figure 1.

We selected five streamflow stations (Mancherial, Tekra, Pathagudam, Perur, and Polavaram; Figure 1a) for our analysis, which are located at major river reaches of the Godavari River. The Mancherial, Tekra, and Pathagudam stations are on reaches that drain into the reach measured by the Perur station, which in turn~~,~~ drains into the Polavaram station. Based on ~~the area of~~ catchment area, Pathagudam is the smallest sub-basin ~~with~~at around 35,625 km^2 ~~area~~, followed by Mancherial (84,375 km^2), Tekra (90,625 km^2), and Perur (226,250 km^2~~) sub-basins.~~). Polavaram is the largest sub-basin, covering approximately 257,500 km².

3. Data and methods

3.1. Observed data

We used ~~the~~ daily meteorological forcing for hydrological ~~modeling~~modelling to simulate ~~the~~ streamflow from 1967~~-~~ to 2019 ~~over~~in the Godavari River basin. Daily precipitation, minimum and maximum temperature, and wind speed datasets were used to develop the daily meteorological forcing. We obtained daily 0.25º gridded observed precipitation data from the India Meteorological Department [IMD, (Pai et al., 2014)]. IMD developed daily gridded precipitation data at 0.25º spatial resolution using the approximately 6995 stations located across the country using the inverse distance weighted interpolation scheme (Pai et al., 2015). Daily maximum and minimum temperature data were also obtained from the IMD at 1º spatial resolution based on 395 stations located across India (Srivastava et al., 2009). To maintain consistency in spatial resolution, maximum and minimum temperature data were regridded ~~at~~to 0.25º using a lapse~~-~~rate relationship and digital elevation model (DEM) described by Maurer et al.

(2002). The precipitation and temperature data from the IMD capture ~~the~~ spatial and temporal variability well across India and have been ~~used~~ widely used in previous studies ~~(Chawla and Mujumdar, 2015; Garg and Mishra, 2019; Mahto and Mishra, 2019; Rajeevan et al., 2012; Shah and Mishra, 2016)~~(Chawla and Mujumdar, 2015; Garg and Mishra, 2019; Mahto and Mishra, 2019; Rajeevan et al., 2012; Shah and Mishra, 2016). The gridded wind data is not available from IMD. Therefore, we collected reanalysis wind speed data from the National Centers for Environmental Prediction- National Center for Atmospheric Research (NCEP-NCAR), which is available at 0.25º spatial resolution. Daily streamflow discharge data for model calibration and validation were obtained from the Central Water Commission (CWC) for the five selected gauging stations (Mancherial, Tekra, Pathagudam, Perur, and Polavaram), for the period 1967-2014. Streamflow data after 2014 have too many gaps and therefore could not be used for our analysis.

3.2. The Variable Infiltration Capacity (VIC) and routing models

The VIC model (Cherkauer et al., 2003; Cherkauer and Lettenmaier, 1999; Liang et al., 1996, 1994) is a physically based, land surface, grid-based hydrologic model that simulates energy and water fluxes at daily and sub-daily timescales for each grid cell (Gao et al., 2010). The hydrological model considers ~~the~~ soil ~~parameters,~~and vegetation parameters, including their sub-grid variability, and meteorological forcing (precipitation, maximum and minimum temperature, and wind speed data) to simulate surface runoff, baseflow, evaporation, and soil moisture. The sub-grid variability of soil and vegetation makes the VIC model more realistic than other physically-based models in heterogeneous topographic regions (Gao et al., 2012). Vegetation parameters for the VIC model were

extracted from the Advanced Very High-Resolution Radiometer (AVHRR) global land-cover information, which is available at 1km spatial resolution (Hansen et al., 2000; Sheffield and Wood, 2007). We used the Harmonized World Soil Database [HWSD; (Fischer et al., 2008)] soil data to develop soil parameters for the VIC model. For the given parameters and meteorological data, the VIC model uses the Xinanjiang model (Ren-Jun, 1992) and Richard's equation (Liang et al., 1994) to estimate the runoff and soil moisture, respectively. VIC considers three layers of soil. Out of the three, only the top two soil layers contribute to the estimation of surface runoff, while the bottom layer contributes to baseflow estimation.

Along with the VIC model, the stand-alone routing model from Lohmann et al., (1996) was used to route surface runoff and baseflow simulated by the VIC to desired locations over the basin. The model is based on two parts, routing within a grid cell and channel routing, where the first uses the unit hydrograph method while the second is performed using the linearized Saint-Venant equation. Both parts of the routing model are developed using the simple linear transfer function (Gao et al., 2010). The streamflow routing model assumes that surface runoff and baseflow exit a cell in a single flow direction ~~based on~~, determined by the topography. Basin and sub-basin delineation and flow direction were computed from the Shuttle Radar Topography Mission elevation data (Digital Object Identifier (DOI) number: /10.5066/F7PR7TFT) for the routing model.

We used the previously calibrated VIC model of the Godavari River basin from Garg and Mishra (2019). Garg and Mishra (2019) calibrated the VIC model using the six soil parameters: Ds_{max} (maximum velocity of baseflow), Ds (Fraction of Ds_{max} where nonlinear baseflow begins), W_s (fraction of the maximum soil moisture where nonlinear

baseflow occurs), b_{inf} (shape of the variable infiltration capacity curve), and soil depths of the second and third layers; which control surface runoff, baseflow, evaporation (in bare soil), and soil moisture in the VIC model. The infiltration shape parameter (b_{inf}) and soil depths are used in the estimation of surface runoff, infiltration, soil moisture, and bare soil evaporation, while $Ds_{max,}$ Ds, and W_s parameters are mainly used for baseflow estimation. More information on the VIC model, input datasets, and parameters can be obtained from Gao et al., (2010) and the Land Surface Hydrology Research Group at the University of Washington (http://uw-hydro.github.io/).

In this study, the calibrated VIC model (Garg and Mishra, 2019) was re-evaluated for the five stations using the updated observed daily streamflow data (~~Figure~~Figures S2-S3, Table S1, S2). We re-evaluated the model performance for the Mancherial, Tekra, Pathagudam, Perur, and Polavaram stations of the Godavari River basins for the 1970-2014 period, where the first 10 years are the calibration period (Garg and Mishra, 2019) and the rest is the validation period (Figure S2, Table S1). The model performance was evaluated using the Nash–Sutcliffe efficiency [NSE; (Nash and Sutcliffe, 1970)], the coefficient of determination (R^2), and bias percentage at low (Bias_Q_5), mean (Bias_mean), and high (Bias_Q_{95}) streamflow values. These metrics (NSE, R^2, and Bias ~~values~~) show that the VIC model performs satisfactorily during the calibration period (Table S1, Figure S2~~) and~~), has ~~an~~ acceptable performance during the validation period (Table S2, Figure S2), and maintains an acceptable performance across different flood years (Figure S3).

In the present study, we did not consider the interventions of human activities in the water cycle due to the limited availability of human intervention datasets. However,

human activities in the basin do not affect ~~the~~ natural river flow in ~~the majority of~~most sub-basins, except ~~for~~in the semi-arid region of the Mancherial sub-basin. A large number of reservoirs were constructed for water storage in this region, which affected the model performance, mostly after 1994. Therefore, the validation period was limited to 1980-1993 for the Mancherial station (Figure S2, Table S2). Such effects were not ~~found in~~observed at the downstream stations of Perur and Polavaram, since the streamflow ~~volume~~ contribution of the semi-arid Mancherial basin is low relative to the rest of the ~~basin area of these two~~ basins. Overall, our results showed that the VIC ~~-~~simulated natural streamflow compares well ~~against~~with the observed daily streamflow for all five stations during the calibration and validation ~~period (Figure~~periods and across different flood events (Figures S2~~, Table~~ and S3, Tables S1~~,~~ and S2). Therefore, the use of VIC (without human intervention) simulated streamflow is acceptable for our analysis.

3.3. Flood event characterization

To understand the flood generation mechanism, we evaluated two major aspects over the Godavari river basin (Figure 2): (i) temporal properties of flood-causing precipitation and surface runoff, and (ii) flood-dominating catchment area.

These analyses were based on observed precipitation data and VIC-simulated runoff and streamflow data. As the focus here is on floods, we identified independent high-streamflow events using the peak-over-threshold approach. First, we selected ~~the~~ daily streamflow ~~discharge more than~~exceeding the 95th percentile threshold ~~value~~ to ~~determine the~~identify high-streamflow events. Later, we grouped the events that occurred

with less than 10 days of separation (Brunner et al., 2020a, 2020b; Diederen et al., 2019) to identify the independent high-streamflow event. If two or more high-streamflow events occurred together within each separation (within 10 days), we used the highest discharge value to make the event independent.

3.3.1. Temporal properties of flood-causing precipitation and surface runoff

Based on the duration of precipitation that leads to flood events, the events can be classified into long or short rain flood types (Berghuijs et al., 2016; Merz and Blöschl, 2003). Accordingly, we performed a temporal analysis of precipitation and runoff to identify the flood types. The correlation between the event peak discharge and basin area-averaged accumulated precipitation (before the peak streamflow) for different durations (range of 1-20 days) and lag times (0-7 days, representing the lag between the end of the precipitation window and the day of the peak streamflow) was estimated for all five sub-basins. A similar analysis was conducted by correlating the event peak discharge with ~~accumulated~~the mean surface runoff prior to the peak.

The precipitation in the time windows found most correlated with the peak discharge was further analyzed to identify three flood-generation storylines, following the studies by Keller et al., (2017) and Berghuijs et al., (2016): (i) flood caused by a single high-intensity precipitation day; (ii) flood caused by multiple high-intensity precipitation days; and (iii) floods caused by low-to-medium intensity precipitation days. For this, we ~~checked~~counted the number of high-precipitation days (above 99th percentile) within the relevant window prior to the flood event. If the number is one, it is identified as caused by a single high precipitation day. If it is more than one, then the flood event is caused by multiple high-intensity precipitation days. Finally, if both conditions fail and there is no

high-precipitation day prior to the flood, then the flood event is caused by multiple low-to-medium intensity precipitation days.

3.3.2. Flood-dominating catchment area

Next, we evaluated the dominated catchment area in flood generation by examining the spatial variability of precipitation and runoff ~~spatial variability~~ (Figure 2). For that, we used the empirical orthogonal function (EOF) analysis and obtained the leading modes of spatial variability in precipitation and surface runoff (Mishra et al., 2012). EOF analysis identifies the dominant modes of spatio-temporal variability in a dataset by solving an eigenvalue problem derived from the spatio-temporal covariance matrix (Lorenz, 1956; Preisendorfer, 1988; Wilks, 2006; Navarra and Simoncini, 2010; Joliffe, 1986; Hannachi, 2022). Here, we first estimated the dominant spatiotemporal modes of variability in the gridded precipitation (surface runoff) to assess its coupling with peak discharge. To do so, we formed the spatial covariance matrix of N x N (where N is the number of grid points) using the following equation:

$$C = \frac{1}{t-1} P' P'^{T}$$

where P' is precipitation (runoff) anomaly; t is the number of peak events; and T represents the transpose matrix.

Further, the spatial covariance matrix (C) was decomposed as:

$$C e_k = \lambda_k e_k$$

where e_k and λ_k are the k^{th} spatial EOF and its associated eigenvalue, respectively (Lorenz, 1956). The fraction of total variance explained by each mode is $\lambda_k / \Sigma\lambda_j$. We also

obtained the Principal Component (PC) time series by projecting the anomaly field onto each EOF:

$$a_k(t) = \sum_{i=1}^{N} P'_{i,t} \cdot e_{k,i}$$

Finally, the coupling between each PC time series and the peak discharge anomaly was quantified using the Pearson correlation coefficient. In the EOF analysis, we used ~~the~~ accumulated precipitation and mean surface runoff at each pixel for the time windows ~~found~~that were most strongly correlated with peak discharge, ~~according to the findings~~as identified in step 1 above.

Lastly, we examine the role of antecedent soil moisture conditions in the runoff generation mechanism. We categorize all flood events into dry and wet conditions based on the soil moisture simulated for the ~~first~~ soil layer (top 60 cm) before the time window found most correlated with peak discharge. ~~If~~The 75th percentile threshold is computed considering all occurrences of the same calendar day across the study period (1967–2019). If soil moisture ~~is more than 75th percentile~~exceeds this threshold, the flood event is identified as a wet condition ~~or vice versa.~~; otherwise, it is identified as a dry condition. Thereafter, we analyzed the mean runoff coefficient (surface runoff divided by precipitation) ~~for~~under wet and dry conditions ~~for~~over the time window found in step 1.

Formatted: Left

Formatted: Font: Times New Roman

Formatted: Font: Times New Roman

Formatted: Font: Times New Roman

4. Results

4.1. High-intensity precipitation and Discharge Flood events

Using the daily precipitation and simulated discharge data, we estimated the high-intensity precipitation and streamflow values (precipitation and discharge values above 95th percentile; P_{95} and Q_{95}) for each month at the Mancherial, Tekra, Pathagudam, Perur, and Polavaram stations, considering the 95th percentile threshold value of the period 1967-2019 (Figure ~~S3~~S4). The majority of high-intensity precipitation (P_{95}) and streamflow (Q_{95}) occurred during the monsoon months (June-September; Figure S3a-e). The ratio of high-intensity streamflow ~~and~~to precipitation ~~values~~ varies ~~with~~over time. The early months of monsoon (i.e., June and July) have a low ratio of Q_{95} and P_{95} compared to late monsoon months (i.e., August and September). Due to initially dry ~~initial~~ soil moisture conditions, most of the ~~majority of~~ high-intensity precipitation that occurred in June and July did not ~~cause~~produce high streamflow in the Godavari River. However, most high-intensity precipitation events ~~cause~~lead to high streamflow in August and September due to wet soil moisture conditions ~~in~~during the late monsoon season (Figure ~~S3~~S4). Moreover, we ~~noticed a~~observed higher ~~ratio of~~ Q_{95} and P_{95} ratios in October in the Mancherial sub-basin, which is associated with wet ~~moisture~~ conditions and the onset of the Northeast monsoon in the sub-basin (Mishra et al., 2021; Rajeevan et al., 2012a). Our preliminary analysis indicates ~~the~~a significant role of high-intensity precipitation and antecedent soil moisture conditions in the occurrence of high-intensity streamflow ~~occurrence~~ over the Godavari basin, ~~which is~~ consistent with the previous study ~~of~~by Garg and Mishra (2019).

To further understand the role of high-intensity precipitation and runoff in basin floods, we first~~, we~~ identified flood events (independent high streamflow events, as described in the method section) for each sub-basin during the period 1967-2019 (Figure 3a). We

found a total of 116, 107, 88, 105, and 104 independent high-streamflow events ~~in~~at the Mancherial, Tekra, Pathagudam, Perur, and Polavaram stations, respectively, during the period 1967-2019 (Figure 3a). Using the identified flood events, we analyzed the temporal and spatial variability of precipitation and runoff in further analysis to understand the attribution of hydrometeorological variables and catchment area to flood generation.

4.2. Temporal properties of flood-causing precipitation and surface runoff

Next, we analyzed the temporal properties of precipitation before the peak streamflow of flood events. We found (Table 1, ~~Table~~Tables S3-S7) that the highest correlation between ~~the~~ basin-averaged accumulated precipitation and ~~the~~ peak streamflow is for lags of 1-2 days and durations that vary between stations. Floods in the semi-arid Mancherial sub-basins were linked ~~with~~to short-duration (2 days) precipitation events (Table S3~~)~~), while floods ~~at~~in other sub-basins (Tekra, Pathagudam, Perur, and Polavaram~~,~~; Tables S4-S7) were well correlated ~~well~~ with long-duration (10-11 days) precipitation. Similarly, we analyzed the temporal dynamics of surface runoff before the occurrence of peak streamflow (Table 2, Tables S8-S12). As expected, the Mancherial sub-basin showed the highest correlation with short-duration (2 days) ~~accumulated~~mean runoff, ~~while~~whereas for the other sub-basins, the highest correlation was ~~found~~ with long-duration (7-8 days) ~~accumulated~~mean runoff (Table 2). The temporal properties of surface runoff are similar to those of precipitation but with a ~~smaller~~shorter time window, ~~which is~~ due to ~~the depletion of~~ some ~~of the~~ precipitation ~~into~~being stored in soil ~~storage~~. Overall, we found that the floods in large parts of the Godavari basin are associated with long-duration precipitation and surface runoff, except ~~for~~in the semi-arid Mancherial sub-

basin, where ~~the~~ floods are characterized by short-duration precipitation and surface runoff (Tables 1~~,~~ ~~-~~2).

The precipitation ~~in~~over the time window presented above was further analyzed for the three different conditions (see Section 3.3.1). We found that for four out of five sub-basins (Tekra, Pathagudam, Perur, and Polavaram), the majority of flood events (around 40-50%) occurred due to multiple high-intensity precipitation (more than 99th percentile) days (Figure 3b). However, most of the floods in the semi-arid Mancherial sub-basin ~~occurred due to~~resulted from single high-intensity precipitation ~~days~~events (Figure 3b). This is not surprising, given the shorter precipitation duration found for Mancherial compared to the other sub-basins. We also found that around 30-40% flood events in Mancherial, Perur, and Polavaram sub-basins are associated with long-term low-intensity precipitation (Figure 3b). Overall, our results showed that the majority of flood events in the semi-humid Tekra, Pathagudam, Perur, and Polavaram sub-basins occurred due to the higher attribution of multiple high-intensity precipitation days. However, the majority of flood events in the semi-arid Mancherial sub-basin occurred due to higher attribution of single-day high-intensity precipitation (Figure 3, Table 1, 2).

4.3. Flood-dominating catchment area

Next, we identify the catchment area, which dominantly contributes to the flood generation mechanism. The flood-dominating catchment area is identified based on the spatial variability of hydrometeorological variables (precipitation and surface runoff patterns) and catchment conditions before the peak streamflow. Using the EOF analysis, we estimated the leading spatial patterns of variability in the accumulated precipitation and mean surface runoff before the peak streamflow, where accumulation of precipitation

and mean runoff was based on the time-windows estimated in the previous analysis (i.e., 2, 10, and 11 days for precipitation and 2, 7, and 8 days for runoff, Tables 1, 2).

Based on the EOF analysis, we ~~found that flood-causing~~captured the dominant pattern of accumulated precipitation ~~occurred predominantly~~during the flood events. We found that floods in ~~downstream areas of~~ the Mancherial and Tekra sub-basins are associated with precipitation occurring over the downstream areas of these sub-basins, which ~~reside~~are located in the central part of the Godavari basin (Figure 4a-c). However, the leading spatial pattern (Mode-1) of accumulated precipitation covers the entire region of Pathagudam (Figure 4a-c). The Perur sub-basin also showed a similar spatial pattern ~~of~~in the EOF analysis for ~~the~~ 10 and 11 days of accumulated precipitation and indicated ~~the~~ high weightage over the central and downstream parts of the sub-~~basins~~basin during flood generation (Figure 4e-h). For the Polavaram sub-basin, we found a high dominance of the central and downstream part of the Godavari basin in the flooding mechanism (Figure 4i-k). Moreover, the correlation between peak streamflow and the leading mode (mode-1) of 10 or 11 days of accumulated precipitation is higher at Tekra, Pathagudam, Perur, and Polavaram sub-basins than the leading mode of 2 days of accumulated precipitation in the same basins (Figure 4d) due to long-rain type floods ~~at Tekra, Pathagudam, Perur, and Polavaram sub-basins~~ (Table 1). Furthermore, EOF analysis ~~for accumulated~~of mean surface runoff (Figure 5) showed a similar leading spatial pattern, although ~~its~~the area is slightly smaller ~~compared to the~~ than that of precipitation (Figure 4). ~~Other than~~ In addition to EOF analysis, we ~~also~~ computed ~~the~~ pixel-based ~~correlation~~correlations between accumulated precipitation and peak streamflow (Figure ~~S4)~~S5), and between ~~accumulated~~mean runoff and peak streamflow (Figure S5), for each

sub-basin over the relevant duration. Our results showed spatial ~~patterns of~~ correlation ~~analysis that were~~ patterns similar to those obtained from the EOF analysis. In addition, our analysis (Figure ~~S4~~S5 and Figure ~~S5~~S6) confirms the previous finding (Figure 4 and Figure 5) where higher correlations of peak streamflow in the Tekra, Pathagudam, Perur, and Polavaram sub-basins are with long-duration precipitation and runoff, compared to short-duration, while for the Mancherial station, the opposite behavior was found.

We further estimated the pixel-based runoff coefficient (ratio of surface runoff to precipitation) before ~~the~~ peak streamflow for 2, 7, and 8 days durations under both dry and wet soil moisture conditions (Figure 6). We found that the Tekra basin showed the highest ~~values of~~ runoff coefficient values compared to ~~the~~ other parts of the basin for all durations and ~~in~~under both wet and dry conditions (Figure 6), indicating the dominance of the Tekra sub-basin in ~~the~~ Godavari ~~river~~River flooding. We also found that the variation in runoff coefficient ~~among~~across durations is lower ~~during the~~under dry conditions ~~compared to the~~than under wet conditions (Figure 6). For instance, under wet conditions, the ~~values of the~~ runoff coefficient values are higher for the 2 days duration and decrease slightly for the 7 and 8 ~~day~~ days durations. The decrease in runoff coefficient for 7 and 8 days durations is due to the lower intensity of rainfall in a long-time span compared to 2 days duration rainfall. However, we found that runoff coefficient values are quite similar ~~for~~across all durations under ~~the~~ dry ~~condition~~conditions. Overall, our results highlight the flood-dominated area of the Godavari basin based on the hydrometeorology and catchment properties. Our analysis reveals that the central region of the Godavari basin and the Tekra sub-basin contribute

significantly to flood generation, compared to other parts of the basin. Furthermore, these results can be used for flood management in the basin.

5. Discussion and Conclusions

Floods pose severe challenges to the infrastructure, ecology, and socio-economic development of the largely populated Indian Subcontinent. Moreover, the risk of floods has increased significantly under global warming (Ali et al., 2019; Arnell and Gosling, 2016; Dottori et al., 2018; Hirabayashi et al., 2013; Milly et al., 2002). Thus, ~~an effort is~~efforts are required to better understand flood~~-~~generation mechanisms in the large river basins of the Indian Subcontinent during the monsoonal climate ~~for~~to support effective flood management. In this study, we examined the temporal and spatial variability of hydrometeorological variables to identify the dominant flood-generating mechanisms and flood-contributing areas using the observed and VIC-simulated hydrological variables~~-~~.

In our analysis, we considered two hydrometeorological variables, precipitation and surface runoff, across the basin to evaluate the flood~~-~~generation mechanism ~~where~~, in which high-intensity precipitation is the primary driver ~~in the~~of flood occurrence. However, previous studies ~~(Garg and Mishra, 2019; Sharma et al., 2018) showed that high-intensity precipitation and floods are not always linked due to pre-hydrological conditions over the catchment.~~(Garg and Mishra, 2019; Sharma et al., 2018; Sharma and Mujumdar, 2024) showed that high-intensity precipitation and floods are not always linked due to initial hydrological conditions over the catchment. There is only 50 to 70% of high-intensity precipitation, which causes flooding in a basin (Garg and Mishra, 2019;

Wasko and Sharma, 2017). Moreover, Sharma and Mujumdar (2024) showed that baseflow has a substantially stronger influence on flood magnitudes than soil moisture. Our results show that the attribution of high-intensity precipitation to flood generation varies with time. For instance, the majority of high-intensity precipitation events ~~in~~during the late monsoon season (August-September) cause flooding in the Godavari basin (Figure S3) due to wetter soil moisture conditions. Therefore, we used a bottom-up approach in our study to examine the temporal and spatial variability of hydrometeorological variables, i.e., we first identified the flood events, and then precipitation and surface runoff variables before the flood events were evaluated to understand their role in the flooding mechanism.

We evaluated the temporal properties of hydrometeorological variables (precipitation and surface runoff) to identify the flood types and processes (Keller et al., 2018; Merz and Blöschl, 2003) that predominantly occur over the Godavari basin in the monsoonal climate. -We found that the majority of floods in the Godavari basin (except Mancherial Basin) are long-rain type floods (Keller et al., 2018; Merz and Blöschl, 2003), which are associated with the 10 to 11 (7 to 8) days long precipitation (mean surface runoff) with multiple high-intensity precipitation events. However, the majority of floods in the semi-arid Mancherial sub-basin are short-rain type. The majority area of the Godavari basin, associated with long-duration precipitation (surface runoff), falls in the semi-humid climate. The rivers in the humid climate can carry a large volume of water (or have a large storage capacity); therefore, a significant amount of rainfall is required for the flood occurrence (Merz and Blöschl, 2003). Previous studies ~~(Hirschboeck et al., 2000; Merz and Blöschl, 2003)~~(Hirschboeck et al., 2000; Merz and

Blöschl, 2003; Nanditha and Mishra, 2022) have found that persistent rainfall in the region is the primary factor in generating long-rain type floods. Consistent with our results, ~~Merz and Blöschl, (2003) showed the long-rain type flood for most humid regions of Austria. Similarly, short-rain type flood in the semi-arid Mancherial region is~~Nandith and Mishra, (2024) showed that Multiday precipitation is the predominant driver of floods over the Indian Subcontinent. Similar to long-rain type floods (associated with humid climate), we observed that the short-rain type floods in the semi-arid Mancherial region are associated with the small storage capacity of the river in the region, which can be easily achieved with shorter rainfall. Therefore, to minimize the risk of flooding in the region, we require a ~~forecast~~forecasting system~~, which~~ that can predict ~~the~~ rainfall for 10 to 11 days duration in the semi-humid climate region.~~-~~ Moreover, we need to understand the occurrence of multiple concurrent extreme precipitation events in the future changing climate.

While the temporal properties of hydrometeorological variables have been widely evaluated to identify flood processes (Keller et al., 2018; Merz and Blöschl, 2003; Nanditha and Mishra, 2022), the spatial patterns of ~~hydrometeorology~~hydrometeorological variables and catchment conditions ~~before~~prior to peak streamflow are ~~commonly ignored.~~often overlooked. This study also evaluated the spatial variability of precipitation and surface runoff ~~before~~prior to peak streamflow to delineate the ~~dominating~~dominant flood-generating areas using ~~the~~ EOF and correlation analyses. We showed that ~~the~~ accumulated precipitation (long- or short-duration ~~accumulated) precipitation)~~ and mean surface runoff before peak streamflow ~~dominantly~~predominantly occur over the central and downstream areas of the Godavari

basin, which contribute to ~~the~~ flood generation. ~~Nied et al., (2014) found that the pre-event spatial patterns of hydrometeorological variables are linked with leading moisture transport and weather system patterns in the region. Moreover, the pre-event hydrometeorological patterns are also associated with the soil moisture patterns (Nied el al., 2014). Since the majority of floods in monsoonal climate occur during the wetter soil moisture condition, the soil moisture patterns may not affect the pre-event hydrometeorological patterns.~~

Apart from spatial patterns of precipitation and surface runoff prior to the flood, catchment properties also play an essential role in flood generation. We found that the majority area of the Tekra sub-basin generates more runoff compared to the other sub-basins. The high runoff ratio in the Tekra sub-basin can be associated with various catchment characteristics (such as high slope, conversion of forest ~~crop~~ to cropland (agricultural land cover~~;~~), clay ~~soil~~ dominant soils, etc.) in this semi-humid region, which results in a large fraction of precipitation contributing to the surface runoff and causing flooding in the downstream areas. Previous studies (Boardman et al., 2003; Holman et al., 2003; Lane, 2017; Marc and Robinson, 2007) showed that the high irrigation area, deforestation, and high slope accelerate the runoff generation mechanism, which causes high runoff in the basin.

With a limited understanding of flood processes in the Indian Subcontinent ~~during~~ ~~the~~under monsoonal ~~climate~~conditions, this study initiates a new discussion to better comprehend the mechanisms of flood generation ~~mechanisms~~ in India, aiming to improve flood management. Using the same approach, we can identify the temporal and spatial variability of hydrometeorological variables ~~for the~~in other Indian River basins, which

Formatted: Font: Times New Roman
Formatted: Font: Times New Roman
Formatted: Font: Times New Roman
Formatted: Font: Times New Roman
Formatted: Font: Times New Roman

can be used for numerous flood- control applications. Overall, our findings provide a better insight into the flood generation mechanism over a large river basin of the Indian Subcontinent during the monsoonal climate. Based on our study, we conclude the following:

1. The majority of floods in the Godavari river basin occurred during the monsoon season. However, during the late monsoon, ~~there is a higher~~ the ratio of high flood events to high precipitation events is higher due to wet soil- moisture conditions.
2. Four out of five sub-basins (except the Mancherial sub-basin) showed the dominance of long-duration type floods in the period 1967-2019. Long-duration rainfall (10-11 days) ~~rainfall~~ causes floods in the semi-humid ~~region~~regions of the Tekra, Pathagudam, Perur, and Polavaram sub-basins. However, Floods in the semi-arid Mancherial sub-basin are associated with short-duration (2 days) precipitation and surface runoff.
3. Floods in the Tekra, Pathagudam, Perur, and Polavaram sub-basins predominantly occur due to multiple high-intensity rainfall days. Therefore, long-duration type floods occurred in these sub-basins. Moreover, our analysis revealed that short-duration floods in the semi-arid Mancherial sub-basin are primarily associated with single-day high-intensity precipitation.
4. Based on the EOF and correlation analyses of precipitation and surface runoff, central and downstream areas of the basin dominate in the flood generation mechanism in the Godavari River, which highlights the importance of these areas in flood management in a future warming climate. Moreover, medium-term (10 to

11 days lead) precipitation forecasts in these regions will be useful for flood and reservoir management forecasting.

5. Our analysis also indicated the importance of the Tekra sub-basin in the high runoff generation in the Godavari basin. Due to favorable catchment characteristics, a large fraction of precipitation contributes to the surface runoff in the Tekra sub-basin. Therefore, ~~more~~additional efforts (~~i.~~e.g., afforestation and sustainable infrastructure development) are needed in the Tekra sub-basin ~~for~~to improve flood management in the downstream region.

In the changing climate and land use land cover (urbanization and deforestation), the risk of floods is projected to increase over the Indian Subcontinent (Ali et al., 2019; Gosain et al., 2006; Gupta and Nair, 2011; Rogger et al., 2017; Shah et al., 2019). Moreover, the moisture-holding capacity of the atmosphere increases (Karl and Trenberth, 2003; Kharin et al., 2007) due to a warming climate, which leads to frequent, intense, and more extended extreme precipitation events (Ali et al., 2019, 2014; Roxy et al., 2017; Vittal et al., 2013). Therefore, reliable information on precipitation and runoff forecasts in the basin is crucial for effective flood mitigation. ~~Moreover~~Since floods in semi-humid regions of the Godavari basin result from multiple high-intensity rainfall days, there is a need for high-skill medium-range precipitation forecasting (especially over the central and downstream regions of the basin) to mitigate flood risk in a warming climate. Moreover, a real-time soil moisture monitoring system is required in the Tekra basin (which experiences high runoff during the monsoon season) to mitigate flooding. In addition to a real-time monitoring and forecasting system, significant steps are needed to reduce the rapid runoff generation in the Tekra sub-basin using natural flood management

methods for flood control in the downstream area of the basin (Lane, 2017). For instance, attenuation of surface runoff can be achieved through afforestation (Marc and Robinson, 2007), changes in arable land-use practices (Boardman et al., 2003), reductions in livestock density (Orr and Carling, 2006), and ~~Changes~~changes in tillage practices (Holman et al., 2003). ~~Along with the study of natural drivers of floods, we also have to analyze the role of human activities (intensive agriculture practices, reservoir operation, groundwater depletion, urbanization, etc.) in the occurrence of flood events in the future.~~

The flood-generating mechanisms cannot be fully understood by natural drivers of floods (such as climate) and static catchment attributes alone. The current study does not consider the extensive role of human activities on water resources and the simulation of hydrological components, which can affect the flood-generating mechanisms (flood propagation and attenuation) in the catchment (Boulange et al., 2021; Haddeland et al., 2014). For instance, previous studies (Boulange et al., 2021; Han et al., 2019; Ruan et al., 2024) have shown the roles of human activities and dynamic catchment attributes in flood severity and exposure. Therefore, a similar study can be conducted separately in the future to analyse the role of human activities (intensive agricultural practices, reservoir operations, groundwater depletion, urbanization, etc.) in the occurrence of flood events. Additionally, our study currently considers a limited number of observed streamflow stations (five) on five major tributaries of the Godavari River Basin, which provides only a limited understanding of flood mechanisms at a fine resolution (sub-catchment level) for more robust flood mitigation measures. Based on the availability of long-term streamflow data for other Godavari River streams, we can further improve understanding of flood mechanisms and the dominant catchment-area contribution to flood generation in

the future using the framework discussed in our study. In this study, we used the calibrated-VIC model for streamflow and runoff simulations, which also exhibits several structural and parametric limitations when applied to predict extreme streamflow events (Abdulla and Lettenmaier, 1997; Liang et al., 2003; Tsai et al., 2021). The VIC model simulates runoff using a saturated-excess mechanism (Liang et al., 1994), which underestimates excess runoff and infiltration estimations during intense monsoon events (Beven, 2012). By considering multiple hydrological models (including human influence) for streamflow prediction, we can reduce model limitations and develop a robust understanding of flood-generating mechanisms across India in the future.

6. Acknowledgements:

The first author appreciates the funding support from Anusadhan National Research Foundation (ANRF) under the Startup Research Grant (SRG). The authors acknowledge the data availability from the India Meteorological Department (IMD), National Centers for Environmental Prediction- National Center for Atmospheric Research (NCEP-NCAR), and the Central Water Commission (CWC). The authors also acknowledge Mr. Shailesh Garg and Dr. Vimal Mishra for providing the calibrated soil parameter datasets for the Godavari River.

7. Author contributions:

SA and EM designed the study and wrote the manuscript. SA simulated the VIC model and performed the analysis. UG prepared the figures and partially contributed to the analysis.

8. Competing interests:

Authors declare no competing interests.

9. Data Availability:

All the datasets used in this study can be obtained from the corresponding author.

10. Code Availability:

Data processing scripts can be obtained from the corresponding author.

11. References:

Abdulla, F.A., Lettenmaier, D.P., 1997. Development of regional parameter estimation equations for a macroscale hydrologic model. J. Hydrol. 197, 230–257. https://doi.org/10.1016/S0022-1694(96)03262-3

Ali, H., Mishra, V., Pai, D.S., 2014. Observed and projected urban extreme rainfall events in India. J. Geophys. Res. Atmos. 119, 12,621-12,641. https://doi.org/10.1002/2014JD022264

Ali, H., Modi, P., Mishra, V., 2019. Increased flood risk in Indian sub-continent under the warming climate. Weather Clim. Extrem. 25, 100212. https://doi.org/10.1016/j.wace.2019.100212

Allan, R.P., Soden, B.J., 2007. Large discrepancy between observed and simulated precipitation trends in the ascending and descending branches of the tropical circulation. Geophys. Res. Lett. 34, L18705. https://doi.org/10.1029/2007GL031460

Arnell, N.W., Gosling, S.N., 2016. The impacts of climate change on river flood risk at the global scale. Clim. Change 134, 387–401. https://doi.org/10.1007/s10584-014-1084-5

673 Berghuijs, W.R., Woods, R.A., Hutton, C.J., Sivapalan, M., 2016. Dominant flood
674 generating mechanisms across the United States. Geophys. Res. Lett. 43, 4382–
675 4390. https://doi.org/10.1002/2016GL068070

676 Beven, K., 2012. Rainfall-Runoff Modelling: The Primer, Second Edi. ed, Rainfall-
677 Runoff Modelling: The Primer: Second Edition. Wiley-Blackwell.
678 https://doi.org/10.1002/9781119951001

679 Blöschl, G., Hall, J., Parajka, J., Perdigão, R.A.P., Merz, B., Arheimer, B., Aronica, G.T.,
680 Bilibashi, A., Bonacci, O., Borga, M., Ivan, Č., Castellarin, A., Chirico, G.B., 2017.
681 European floods. Science (80-.). 357, 588–590.
682 https://doi.org/10.1126/science.aan2506

683 Blöschl, G., Nester, T., Komma, J., Parajka, J., Perdigão, R.A.P., 2013. The June 2013
684 flood in the Upper Danube Basin, and comparisons with the 2002, 1954 and 1899
685 floods. Hydrol. Earth Syst. Sci. 17, 5197–5212. https://doi.org/10.5194/HESS-17-
686 5197-2013

687 Boardman, J., Evans, R., Ford, J., 2003. Muddy floods on the South Downs, southern
688 England: problem and responses. Environ. Sci. Policy 6, 69–83.
689 https://doi.org/10.1016/S1462-9011(02)00125-9

690 Boulange, J., Hanasaki, N., Yamazaki, D., Pokhrel, Y., 2021. Role of dams in reducing
691 global flood exposure under climate change. Nat. Commun. 2021 121 12, 1–7.
692 https://doi.org/10.1038/s41467-020-20704-0

693 Brunner, M.I., Gilleland, E., Wood, A., Swain, D.L., Clark, M., 2020a. Spatial
694 Dependence of Floods Shaped by Spatiotemporal Variations in Meteorological and

695 Land-Surface Processes. Geophys. Res. Lett. 47, e2020GL088000.
696 https://doi.org/10.1029/2020GL088000

697 Brunner, M.I., Papalexiou, S., Clark, M.P., Gilleland, E., 2020b. How Probable Is
698 Widespread Flooding in the United States? Water Resour. Res. 56,
699 e2020WR028096. https://doi.org/10.1029/2020WR028096

700 Chawla, I., Mujumdar, P.P., 2015. Isolating the impacts of land use and climate change
701 on streamflow. Hydrol. Earth Syst. Sci. 19, 3633–3651.
702 https://doi.org/10.5194/HESS-19-3633-2015

703 Cherkauer, K.A., Bowling, L.C., Lettenmaier, D.P., 2003. Variable infiltration capacity
704 cold land process model updates. Glob. Planet. Change 38, 151–159.
705 https://doi.org/10.1016/S0921-8181(03)00025-0

706 Cherkauer, K.A., Lettenmaier, D.P., 1999. Hydrologic effects of frozen soils in the upper
707 Mississippi River basin. J. Geophys. Res. Atmos. 104, 19599–19610.
708 https://doi.org/10.1029/1999JD900337

709 Diederen, D., Liu, Y., Gouldby, B., Diermanse, F., Vorogushyn, S., 2019. Stochastic
710 generation of spatially coherent river discharge peaks for continental event-based
711 flood risk assessment. Nat. Hazards Earth Syst. Sci. 19, 1041–1053.
712 https://doi.org/10.5194/NHESS-19-1041-2019

713 Dottori, F., Szewczyk, W., Ciscar, J.-C., Zhao, F., Alfieri, L., Hirabayashi, Y., Bianchi,
714 A., Mongelli, I., Frieler, K., Betts, R.A., Feyen, L., 2018. Increased human and
715 economic losses from river flooding with anthropogenic warming. Nat. Clim.
716 Chang. 8, 781–786. https://doi.org/10.1038/s41558-018-0257-z

717 Fischer, G., Nachtergaele, F., Prieler, S., Velthuizen, H.T. van, Verelst, L., Wiberg, D.,
718 2008. Global Agro-ecological Zones Assessment for Agriculture [WWW
719 Document]. IIASA, Laxenburg, Austria FAO, Rome, Italy. URL
720 https://www.fao.org/soils-portal/data-hub/soil-maps-and-databases/harmonized-
721 world-soil-database-v12/en/

722 Gao, H., Birkett, C., Lettenmaier, D.P., 2012. Global monitoring of large reservoir
723 storage from satellite remote sensing. Water Resour. Res. 48.
724 https://doi.org/10.1029/2012WR012063

725 Gao, H., Tang, Q., Shi, X., Zhu, C., Bohn, T.J., Su, F., Sheffield, J., Pan, M.,
726 Lettenmaier, D.P., Wood, E.F., 2010. Water budget record from Variable Infiltration
727 Capacity (VIC) model. Algorithm Theor. Basis Doc. Terr. Water Cycle Data Rec.

728 Garg, S., Mishra, V., 2019. Role of Extreme Precipitation and Initial Hydrologic
729 Conditions on Floods in Godavari River Basin, India. Water Resour. Res. 55, 9191–
730 9210. https://doi.org/10.1029/2019WR025863

731 Gosain, A.K., Rao, S., Basuray, D., 2006. Climate change impact assessment on
732 hydrology of Indian river basins. Curr. Sci. 90, 346–353.

733 Grams, C.M., Binder, H., Pfahl, S., Piaget, N., Wernli, H., 2014. Atmospheric processes
734 triggering the central European floods in June 2013. Nat. Hazards Earth Syst. Sci.
735 14, 1691–1702. https://doi.org/10.5194/NHESS-14-1691-2014

736 Guerreiro, S.B., Fowler, H.J., Barbero, R., Westra, S., Lenderink, G., Blenkinsop, S.,
737 Lewis, E., Li, X.-F., 2018. Detection of continental-scale intensification of hourly
738 rainfall extremes. Nat. Clim. Chang. 8, 803–807. https://doi.org/10.1038/s41558-

018-0245-3

Gupta, A.K., Nair, S.S., 2011. Urban floods in Bangalore and Chennai: risk management challenges and lessons for sustainable urban ecology. Curr. Sci. 100, 1638–1645.

Haddeland, I., Heinke, J., Biemans, H., Eisner, S., Flörke, M., Hanasaki, N., Konzmann, M., Ludwig, F., Masaki, Y., Schewe, J., Stacke, T., Tessler, Z.D., Wada, Y., Wisser, D., 2014. Global water resources affected by human interventions and climate change. Proc. Natl. Acad. Sci. 111.

Han, Z., Long, D., Fang, Y., Hou, A., Hong, Y., 2019. Impacts of climate change and human activities on the flow regime of the dammed Lancang River in Southwest China. J. Hydrol. 570, 96–105. https://doi.org/10.1016/J.JHYDROL.2018.12.048

Hansen, M.C., DeFries, R.S., Townshend, J.R., Sohlberg, R., 2000. Global land cover classification at 1 km spatial resolution using a classification tree approach. Int. J. Remote Sens. 21, 1331–1364.

Hirabayashi, Y., Mahendran, R., Koirala, S., Konoshima, L., Yamazaki, D., Watanabe, S., Kim, H., Kanae, S., 2013. Global flood risk under climate change. Nat. Clim. Chang. 3, 816–821. https://doi.org/10.1038/nclimate1911

Hirschboeck, K.K., Ely, L., Maddox, R.A., 2000. Hydroclimatology of meteorologic floods, in: Wohl, E. (Ed.), In Inland Flood Hazards: Human, Riparian and AquaticCommunities. Cambridge University Press, New York, pp. 39–72.

Holman, I.P., Hollis, J.M., Bramley, M.E., Thompson, T.R.E., 2003. The contribution of soil structural degradation to catchment flooding: a preliminary investigation of the

760 2000 floods in England and Wales. Hydrol. Earth Syst. Sci. 7, 755–766.
761 https://doi.org/10.5194/HESS-7-755-2003

762 Karl, T.R., Trenberth, K.E., 2003. Modern global climate change. Science 302, 1719–23.
763 https://doi.org/10.1126/science.1090228

764 Keller, L., Rössler, O., Martius, O., Weingartner, R., 2018. Delineation of flood
765 generating processes and their hydrological response. Hydrol. Process. 32, 228–240.
766 https://doi.org/10.1002/HYP.11407

767 Kharin, V. V., Zwiers, F.W., Zhang, X., Hegerl, G.C., 2007. Changes in temperature and
768 precipitation extremes in the IPCC ensemble of global coupled model simulations. J.
769 Clim. 20, 1419–1444.

770 Kundzewicz, Z.W., Kanae, S., Seneviratne, S.I., Handmer, J., Nicholls, N., Peduzzi, P.,
771 Mechler, R., Bouwer, L.M., Arnell, N., Mach, K., Muir-Wood, R., Brakenridge,
772 G.R., Kron, W., Benito, G., Honda, Y., Takahashi, K., Sherstyukov, B., 2014. Flood
773 risk and climate change: global and regional perspectives. Hydrol. Sci. J. 59, 1–28.
774 https://doi.org/10.1080/02626667.2013.857411

775 Lane, S.N., 2017. Natural flood management. WIREs Water 4.
776 https://doi.org/10.1002/WAT2.1211

777 Li, D., Lettenmaier, D.P., Margulis, S.A., Andreadis, K., 2019. The Role of Rain-on-
778 Snow in Flooding Over the Conterminous United States. Water Resour. Res. 55,
779 8492–8513. https://doi.org/10.1029/2019WR024950

780 Liang, X., Lettenmaier, D.P., Wood, E.F., Burges, S.J., 1994. A simple hydrologically

based model of land surface water and energy fluxes for general circulation models. J. Geophys. Res. Atmos. 99, 14415–14428.

Liang, X., Wood, E.F., Lettenmaier, D.P., 1996. Surface soil moisture parameterization of the VIC-2L model: Evaluation and modification. Glob. Planet. Change 13, 195–206.

Liang, X., Xie, Z., Huang, M., 2003. A new parameterization for surface and groundwater interactions and its impact on water budgets with the variable infiltration capacity (VIC) land surface model. J. Geophys. Res. Atmos. 108. https://doi.org/10.1029/2002JD003090;WGROUP:STRING:PUBLICATION

Lindell, M.K., Arlikatti, S., Huang, S.K., 2019. Immediate behavioral response to the June 17, 2013 flash floods in Uttarakhand, North India. Int. J. Disaster Risk Reduct. 34, 129–146. https://doi.org/10.1016/J.IJDRR.2018.11.011

Lohmann, D., NOLTE-HOLUBE, R., RASCHKE, E., 1996. A large-scale horizontal routing model to be coupled to land surface parametrization schemes. Tellus A 48, 708–721. https://doi.org/10.1034/j.1600-0870.1996.t01-3-00009.x

Mahto, S.S., Mishra, V., 2019. Does ERA-5 Outperform Other Reanalysis Products for Hydrologic Applications in India? J. Geophys. Res. Atmos. 124, 9423–9441. https://doi.org/10.1029/2019JD031155

Marc, V., Robinson, M., 2007. The long-term water balance (1972-2004) of upland forestry and grassland at Plynlimon, mid-Wales. Hydrol. Earth Syst. Sci. 11, 44–60. https://doi.org/10.5194/HESS-11-44-2007

802 Maurer, E.P., Wood, A.W., Adam, J.C., Lettenmaier, D.P., 2002. A long-term
803 hydrologically based dataset of land surface fluxes and states for the conterminous
804 United States. Am. Meteorol. Soc. 21, 116–119. https://doi.org/10.1175/JCLI-D-12-
805 00508.1

806 Merz, R., Blöschl, G., 2003. A process typology of regional floods. Water Resour. Res.
807 39, 1340. https://doi.org/10.1029/2002WR001952

808 Milly, P.C.D., Wetherald, R.T., Dunne, K.A., Delworth, T.L., 2002. Increasing risk of
809 gret floods in a changing climate. Nature 415, 514–517.

810 Min, S.-K., Zhang, X., Zwiers, F.W., Hegerl, G.C., 2011. Human contribution to more-
811 intense precipitation extremes. Nature 470. https://doi.org/10.1038/nature09763

812 Mishra, V., Aadhar, S., Shah, H., Kumar, R., Pattanaik, D.R., Tiwari, A.D., 2018. The
813 Kerala flood of 2018: combined impact of extreme rainfall and reservoir storage.
814 Hydrol. Earth Syst. Sci. Discuss. 1–13. https://doi.org/10.5194/hess-2018-480

815 Mishra, V., Smoliak, B. V, Lettenmaier, D.P., Wallace, J.M., 2012. A prominent pattern
816 of year-to-year variability in Indian Summer Monsoon Rainfall. Proc. Natl. Acad.
817 Sci. 109, 7213–7217. https://doi.org/10.1073/pnas.1119150109

818 Mujumdar, G.G., Rajaguru S. N., Pappu R. S., 1969. THE RECENT GODAVARI
819 FLOOD (SEPTEMBER 1969) AND ITS RELEVANCE TO PREHISTORIC
820 ARCHAEOLOGY on JSTOR. Bull. Deccan Coll. Post-Graduate Res. Inst. 29, 118–
821 134.

822 Nageswara Rao, G., 2001. Occurrence of heavy rainfall around the confluence line in

monsoon disturbances and its importance in causing floods. Proc. Indian Acad. Sci. Earth Planet. Sci. 110, 87–94. https://doi.org/10.1007/bf02702232

Nanditha, J.S., Mishra, V., 2024. Projected increase in widespread riverine floods in India under a warming climate. J. Hydrol. 630, 130734. https://doi.org/10.1016/j.jhydrol.2024.130734

Nanditha, J.S., Mishra, V., 2022. Multiday Precipitation Is a Prominent Driver of Floods in Indian River Basins. Water Resour. Res. 58, e2022WR032723. https://doi.org/10.1029/2022WR032723;REQUESTEDJOURNAL:JOURNAL:19447973;WGROUP:STRING:PUBLICATION

Nanditha, J.S., Rajagopalan, B., Mishra, V., 2022. Combined signatures of atmospheric drivers, soil moisture, and moisture source on floods in Narmada River basin, India. Clim. Dyn. 2022 599 59, 2831–2851. https://doi.org/10.1007/S00382-022-06244-X

Nash, J.E., Sutcliffe, J.V., 1970. River flow forecasting through conceptual models part I — A discussion of principles. J. Hydrol. 10, 282–290. https://doi.org/10.1016/0022-1694(70)90255-6

Nied, M., Pardowitz, T., Nissen, K., Ulbrich, U., Hundecha, Y., Merz, B., 2014. On the relationship between hydro-meteorological patterns and flood types. J. Hydrol. 519, 3249–3262. https://doi.org/10.1016/J.JHYDROL.2014.09.089

~~Orr, H.G., Carling, P.A., 2006. Hydro-climatic and land use changes in the River Lune catchment, North West England, implications for catchment management. River Res. Appl. 22, 239–255. https://doi.org/10.1002/RRA.908~~

844 Pai, D.S., Sridhar, L., Badwaik, M.R., Rajeevan, M., 2015. Analysis of the daily rainfall
845 events over India using a new long period (1901–2010) high resolution (0.25° ×
846 0.25°) gridded rainfall data set. Clim. Dyn. 45, 755–776.
847 https://doi.org/10.1007/s00382-014-2307-1

848 Pai, D.S., Sridhar, L., Rajeevan, M., Sreejith, O.P., Satbhai, N.S., Mukhopadhyay, B.,
849 2014. Development of a new high spatial resolution (0.25° × 0.25°) long period
850 (1901-2010) daily gridded rainfall data set over India and its comparison with
851 existing data sets over the region. Mausam 65, 1–18.

852 Rajeevan, M., Unnikrishnan, C.K., Preethi, B., 2012. Evaluation of the ENSEMBLES
853 multi-model seasonal forecasts of Indian summer monsoon variability. Clim. Dyn.
854 38, 2257–2274. https://doi.org/10.1007/s00382-011-1061-x

855 Rakhecha, P., Singh, V., 2017. Enveloping Curves for the Highest Floods of River basins
856 in India. Int. J. Hydrol. 1. https://doi.org/10.15406/ijh.2017.01.00015

857 Rakhecha, P.R., 2002. Highest floods in India. IAHS Publ. 167–172.

858 Ray, K., Pandey, P., Pandey, C., Dimri, A.P., Kishore, K., 2019. On the recent floods in
859 India. Curr. Sci. 117, 204–218.

860 Ren-Jun, Z., 1992. The Xinanjiang model applied in China. J. Hydrol. 135, 371–381.
861 https://doi.org/10.1016/0022-1694(92)90096-E

862 Rogger, M., Agnoletti, M., Alaoui, A., Bathurst, J.C., Bodner, G., Borga, M., Chaplot,
863 V., Gallart, F., Glatzel, G., Hall, J., Holden, J., Holko, L., Horn, R., Kiss, A.,
864 Kohnová, S., Leitinger, G., Lennartz, B., Parajka, J., Perdigão, R., Peth, S.,

Plavcová, L., Quinton, J.N., Robinson, M., Salinas, J.L., Santoro, A., Szolgay, J., Tron, S., Akker, J.J.H. van den, Viglione, A., Blöschl, G., 2017. Land use change impacts on floods at the catchment scale: Challenges and opportunities for future research. Water Resour. Res. 53, 5209–5219. https://doi.org/10.1002/2017WR020723

Roxy, M.K., Ghosh, S., Pathak, A., Athulya, R., Mujumdar, M., Murtugudde, R., Terray, P., Rajeevan, M., 2017. A threefold rise in widespread extreme rain events over central India. Nat. Commun. 8. https://doi.org/10.1038/s41467-017-00744-9

Ruan, Y., Jin, J., Mo, C., Guan, T., Sun, G., Yu, Z., Tang, L., Lei, X., Wang, G., 2024. The combined impact of historical climate change and human activities on reservoir flood control risk. J. Hydrol. Reg. Stud. 52, 101705. https://doi.org/10.1016/J.EJRH.2024.101705

Shah, H.L., Mishra, V., 2016. Hydrologic changes in Indian subcontinental river basins (1901-2012). J. Hydrometeorol. 17, 2667–2687. https://doi.org/10.1175/JHM-D-15-0231.1

Shah, H.L., Zhou, T., Sun, N., Huang, M., Mishra, V., 2019. Roles of Irrigation and Reservoir Operations in Modulating Terrestrial Water and Energy Budgets in the Indian Subcontinental River Basins. J. Geophys. Res. Atmos. 124, 12915–12936. https://doi.org/10.1029/2019JD031059

Sharma, A., Wasko, C., Lettenmaier, D.P., 2018. If Precipitation Extremes Are Increasing, Why Aren't Floods? Water Resour. Res. 54, 8545–8551. https://doi.org/10.1029/2018WR023749

Sharma, S., Mujumdar, P.P., 2024. Baseflow significantly contributes to river floods in Peninsular India. Sci. Reports 2024 141 14, 1251-. https://doi.org/10.1038/s41598-024-51850-w

Sheffield, J., Wood, E.F., 2007. Characteristics of global and regional drought, 1950–2000: Analysis of soil moisture data from off-line simulation of the terrestrial hydrologic cycle. J. Geophys. Res. 112, D17115. https://doi.org/10.1029/2006JD008288

Sikorska, A.E., Viviroli, D., Seibert, J., 2015. Flood-type classification in mountainous catchments using crisp and fuzzy decision trees. Water Resour. Res. 51, 7959–7976. https://doi.org/10.1002/2015WR017326

Srivastava, A.K., Rajeevan, M., Kshirsagar, S.R., 2009. Development of a high resolution daily gridded temperature data set (1969-2005) for the Indian region. Atmos. Sci. Lett. 10, 249–254. https://doi.org/10.1002/asl.232

Tarasova, L., Merz, R., Kiss, A., Basso, S., Blöschl, G., Merz, B., Viglione, A., Plötner, S., Guse, B., Schumann, A., Fischer, S., Ahrens, B., Anwar, F., Bárdossy, A., Bühler, P., Haberlandt, U., Kreibich, H., Krug, A., Lun, D., Müller-Thomy, H., Pidoto, R., Primo, C., Seidel, J., Vorogushyn, S., Wietzke, L., 2019. Causative classification of river flood events. Wiley Interdiscip. Rev. Water 6, e1353. https://doi.org/10.1002/WAT2.1353

The Hindu, 2011. When Bhadrachalam was under a sheet of water. The Hindu.

Trenberth, K.E., Dai, A., Rasmussen, R.M., Parsons, D.B., 2003. The Changing Character of Precipitation. Bull. Am. Meteorol. Soc. 84, 1205–1218.

https://doi.org/10.1175/BAMS-84-9-1205

Tsai, W.P., Feng, D., Pan, M., Beck, H., Lawson, K., Yang, Y., Liu, J., Shen, C., 2021. From calibration to parameter learning: Harnessing the scaling effects of big data in geoscientific modeling. Nat. Commun. 2021 121 12, 5988-. https://doi.org/10.1038/s41467-021-26107-z

Ummenhofer, C.C., Gupta, A. Sen, Li, Y., Taschetto, A.S., England, M.H., 2011. Multi-decadal modulation of the El Niño-Indian monsoon relationship by Indian Ocean variability. Environ. Res. Lett 6, 34006–34014. https://doi.org/10.1088/1748-9326/6/3/034006

Viglione, A., Chirico, G.B., Komma, J., Woods, R., Borga, M., Blöschl, G., 2010. Quantifying space-time dynamics of flood event types. J. Hydrol. 394, 213–229. https://doi.org/10.1016/J.JHYDROL.2010.05.041

Vittal, H., Karmakar, S., Ghosh, S., 2013. Diametric changes in trends and patterns of extreme rainfall over India from pre-1950 to post-1950. Geophys. Res. Lett. 40, 3253–3258. https://doi.org/10.1002/GRL.50631

Wasko, C., Sharma, A., 2017. Global assessment of flood and storm extremes with increased temperatures. Sci. Reports 2017 71 7, 1–8. https://doi.org/10.1038/s41598-017-08481-1

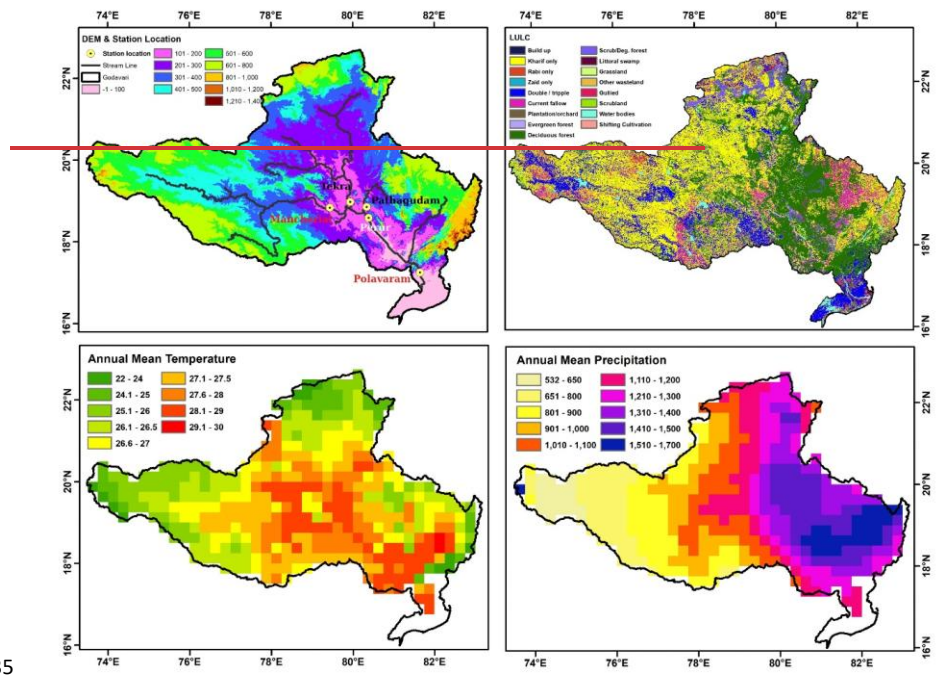
930

931

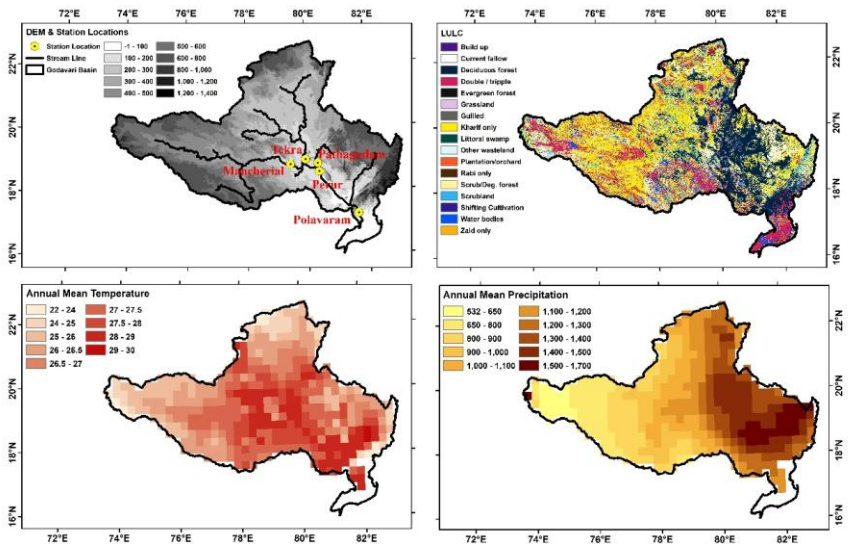
932

933

934 **12. Figures & Tables:**



935



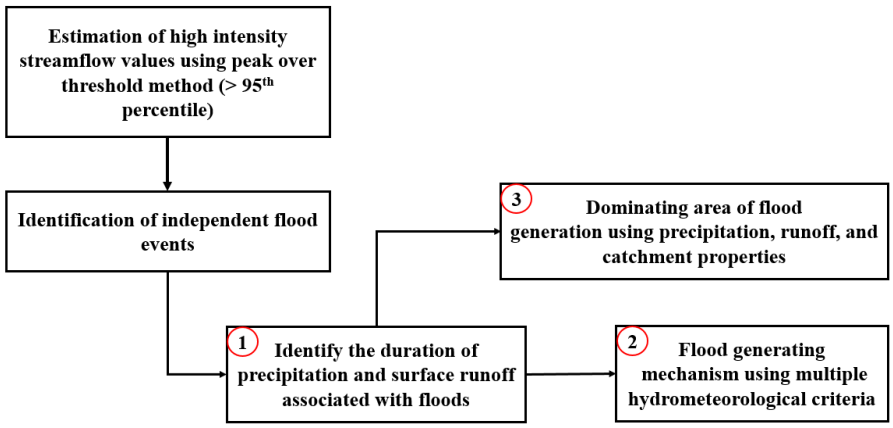
936

937 **Figure 1: Catchment and climate information of the Godavari ~~river~~River.** (a-b)

938 Topographic using the Digital Elevation Map (DEM) and Land use land cover (LULC)

939 information of the Godavari river basin. (c-d) Climate conditions over the basin using the

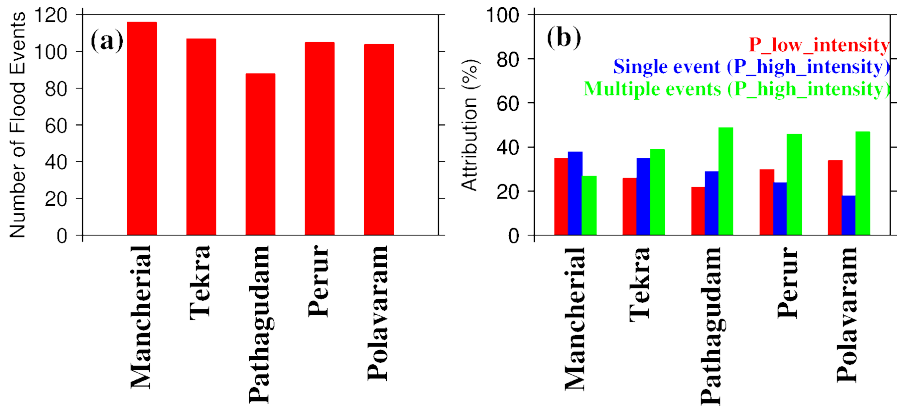
940 annual mean temperature and precipitation during 1967-2019.



941

942 **Figure 2. Major steps used in the analysis.**

943



944

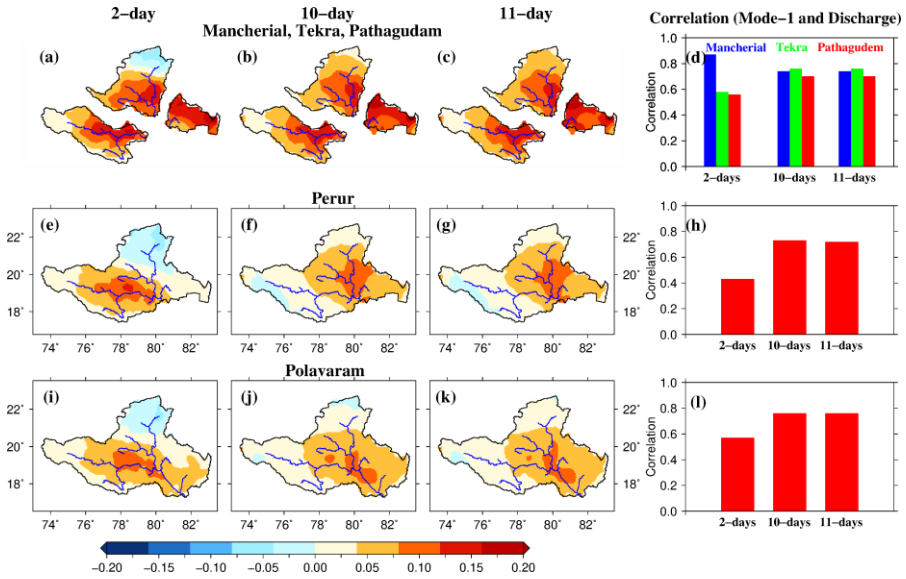
945 **Figure 3. Floods associated with multiple criteria of precipitation over the Godavari**

946 **River Basin.** (a) number of flood events in each sub-basin. (b) Attribution (%) of low-

947 intensity precipitation, single high-intensity precipitation, and multiple days' high-

948 intensity precipitation in flood generation.

949

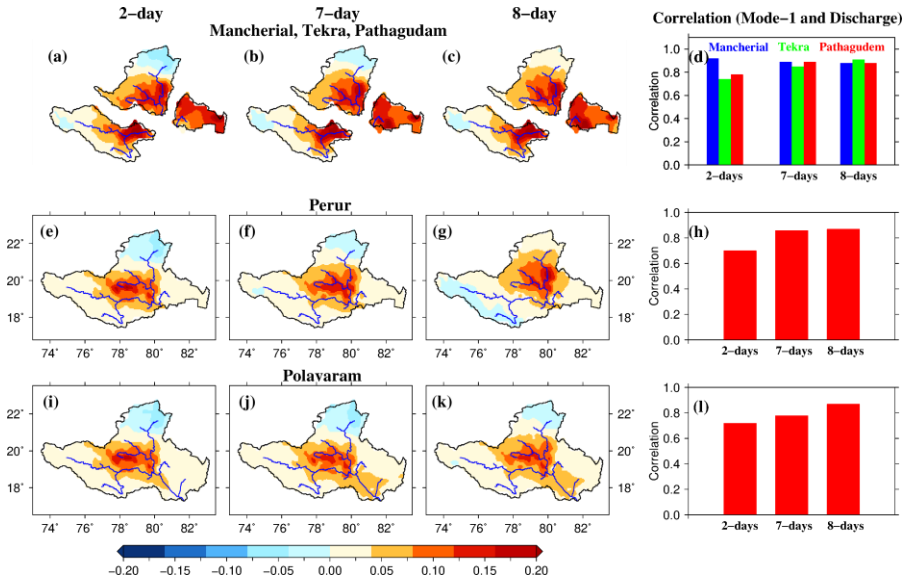


950

951 **Figure 4:** The leading mode of variability in the accumulated precipitation during the high
952 streamflow events for the period 1967-2019 using the method of empirical orthogonal function
953 (EOF). (a-c) The first leading EOF mode of (a) 2- days, (b) 10- days, and (c) 11- days accumulated
954 precipitation for ~~the Polavaram sub-basin.~~Mancherial (left), Tekra (middle), and Pathagudam
955 (right) sub-basins. (d) Correlation between the first leading mode and flood peak at ~~the Polavaram~~
956 ~~station.~~Mancherial (left), Tekra (middle), and Pathagudam (right) stations. (e-h) same as (a-d) but
957 for the Perur sub-basin. (i-l) same as (a-d) but for ~~Mancherial (left), Tekra (middle), and~~
958 ~~Pathagudam (right) sub-basins~~the Polavaram sub-basin.

959

Formatted: Justified



960

961 **Figure 5.** The leading mode of variability in the ~~accumulated~~mean runoff (excess precipitation)
962 during the extreme floods for the period 1967-2019 using the method of empirical orthogonal
963 function (EOF). (a-c) The first leading EOF mode of (a) 2-_days, (b) 7-_days, and (c) 8-_days
964 ~~accumulated~~mean runoff for ~~Polavaram sub-basin.~~Mancherial (left), Tekra (middle), and
965 Pathagudam (right) sub-basins. (d) Correlation between the first leading ~~principle~~principal
966 component (PC-1) and extreme floods ~~over at Polavaram station~~at Mancherial (left), Tekra
967 (middle), and Pathagudam (right) stations during 1967-2019 for 2, 7, and 8-_days ~~accumulated~~mean
968 runoff. (e-h) same as (a-d) but for the Perur sub-basin. (i-l) same as (a-d) but for ~~Mancherial (left),~~
969 ~~Tekra (middle), and Pathagudam (right) sub-basins~~the Polavaram sub-basin.

970

Formatted: Justified

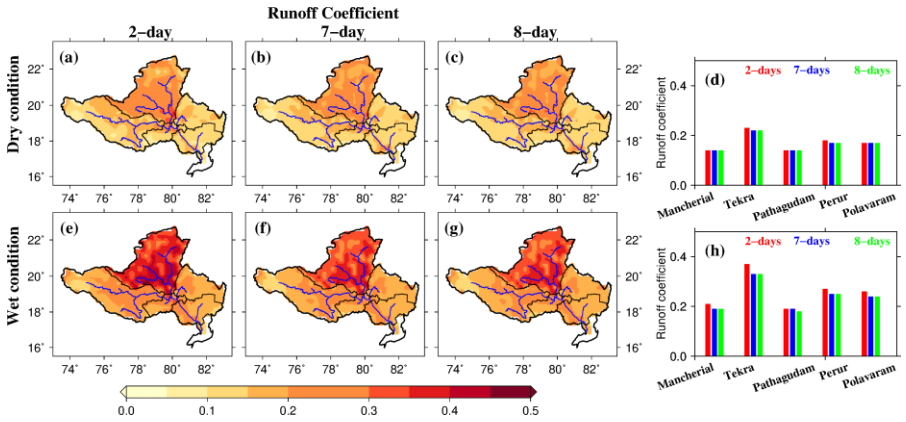


Figure 6. Runoff coefficient over the Godavari basin during the flood events in the period 1967-2019. (a-c) Variability in runoff coefficient values using (a) 2- days, (b) 7- days, and (c) 8- days cumulative precipitation and mean runoff during dry condition flood events. (~~d-f~~e-g) Similar to (a-c~~)~~), but with variability in runoff coefficient values during wet condition flood events.

Formatted: Justified

Table 1: Duration and lag (days) where the basin-averaged accumulated precipitation has the highest correlation with simulated flood peak for high streamflow events at different stations.

Station	Lag-time	Duration
Mancherial	2	2
Tekra	1	11
Pathagudam	2	10

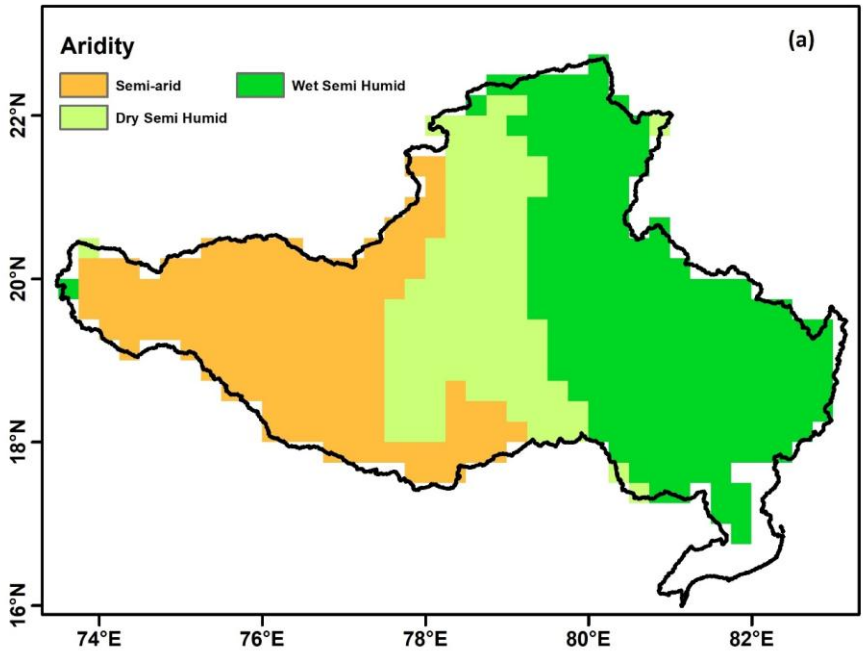
Perur	2	10
Polavaram	2	11

Table 2: Duration and lag (days) where the basin-averaged simulated ~~accumulated~~mean surface runoff has the highest correlation with the simulated flood peak for high streamflow events at different stations

Station	**Lag-time**	**Duration**
Mancherial	2	2
Tekra	1	8
Pathagudam	2	7
Perur	2	7
Polavaram	2	7

994

995 **Supplemental Figures and Tables:**



996

997 Figure S1. Climatic zones in the Godavari Basin using the aridity Index (AI = mean
998 annual precipitation/mean annual PET). Climate zones are classified as semiarid ($0.2 \leq$
999 $AI < 0.5$), dry semi-humid ($0.5 \leq AI < 0.65$), and wet semi-humid ($0.65 \leq AI < 1.33$)
1000 regions.

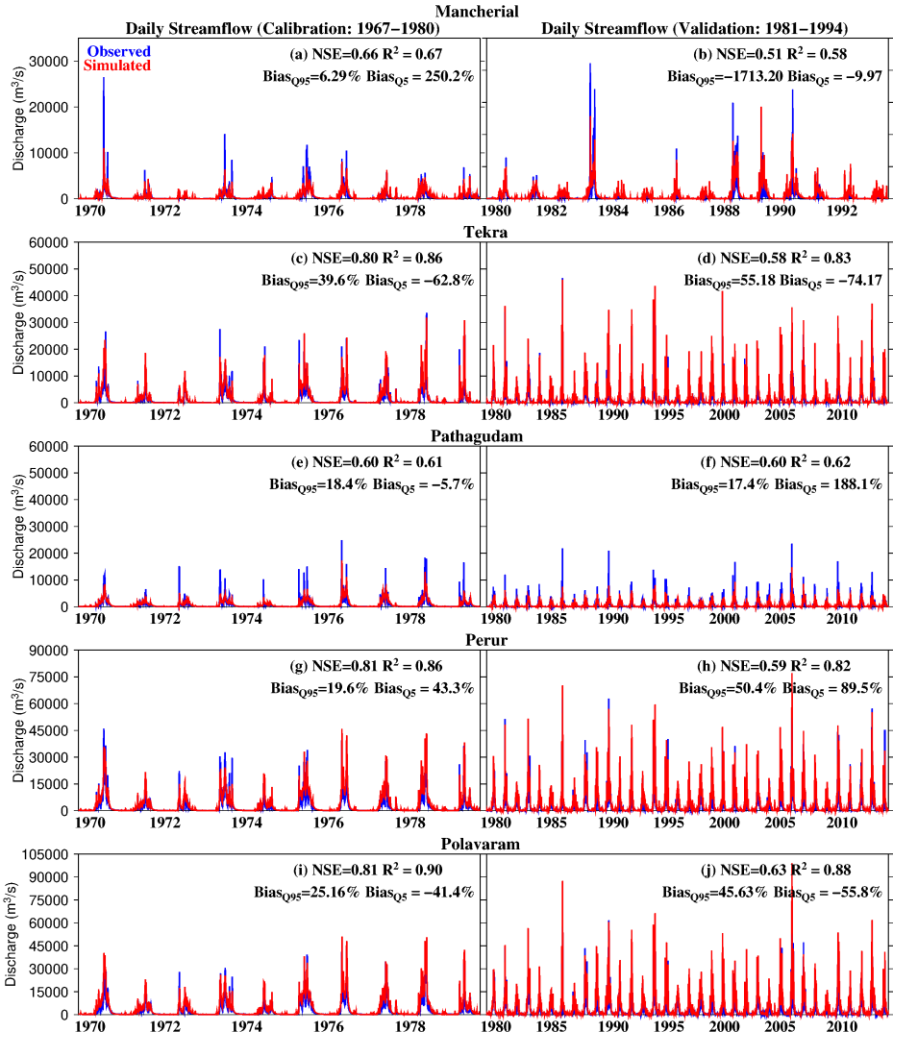
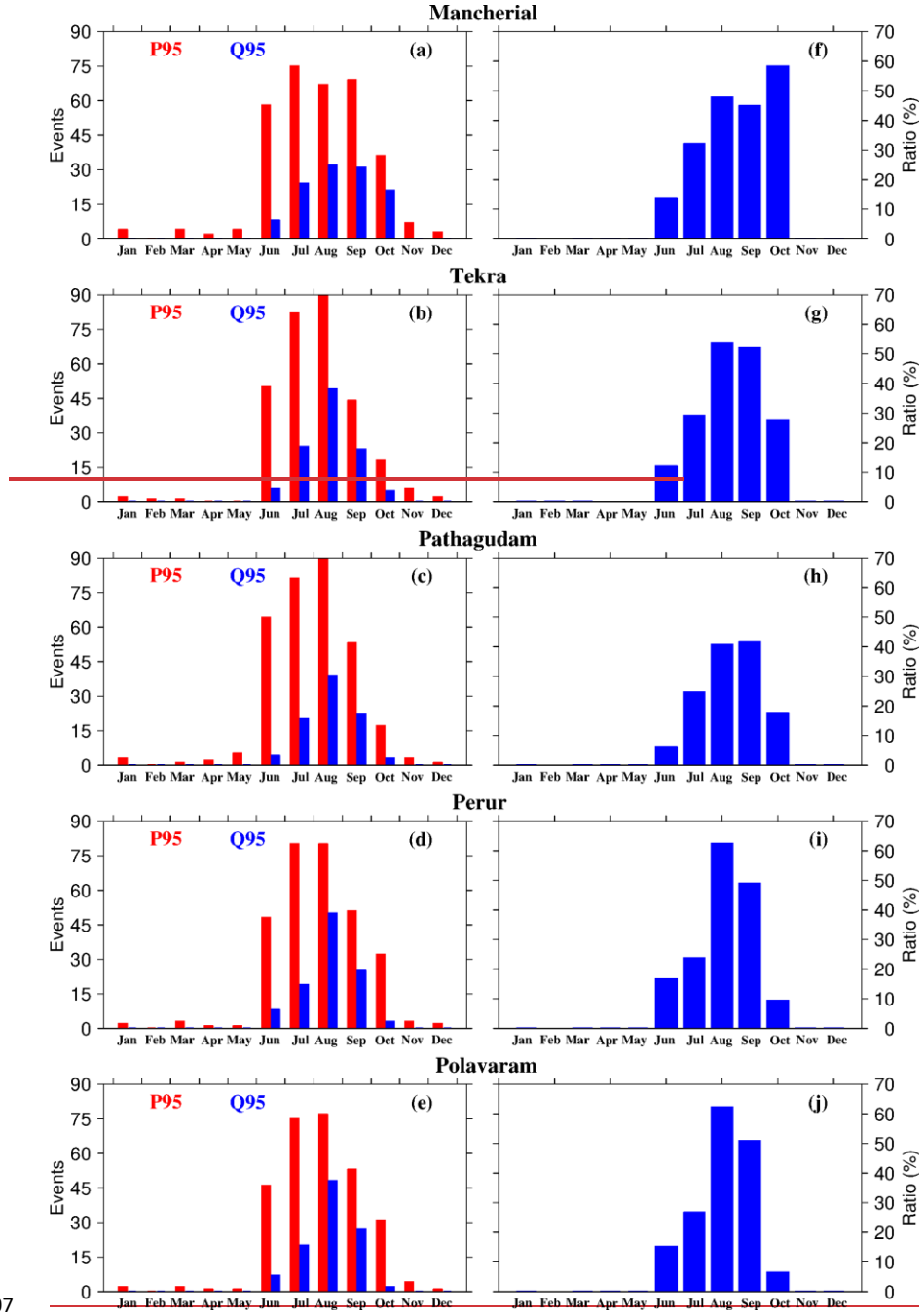


Figure S2. Calibration and validation of the VIC model-simulated streamflow against observed streamflow data at Mancherial, Tekra, Pathagudam, Perur, and Polavaram, for the period 1970-2014. The model was calibrated for the period 1970-1979 and validated for the period 1980-2014 (except for the Mancherial station, which was validated for 1980-1993).


Mancherial
Tekra
Pathagudam
Perur
Polavaram
P95
Q95
(a)
(b)
(c)
(d)
(e)
(f)
(g)
(h)
(i)
(j)
Events
Ratio (%)
Jan Feb Mar Apr May Jun Jul Aug Sep Oct Nov Dec

1007

~~Figure S3.~~

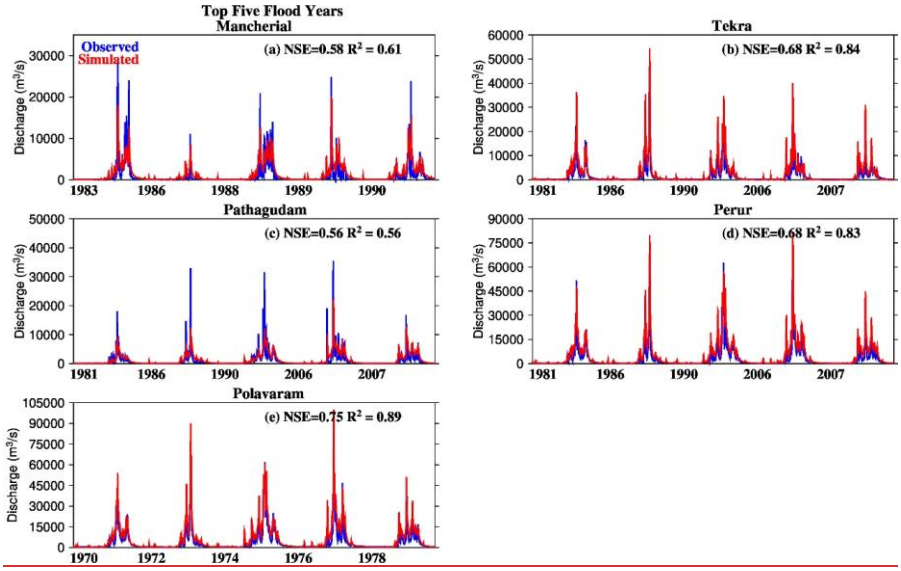


Figure S3. (a–e) Comparison of daily observed (blue) and VIC- simulated (red) streamflow (m^3/s) for the top five major flood years at Mancherial, Tekra, Pathagudam, Perur, and Polavaram during the validation period 1980-2014 (except for the Mancherial station, which was validated for 1980-1993).

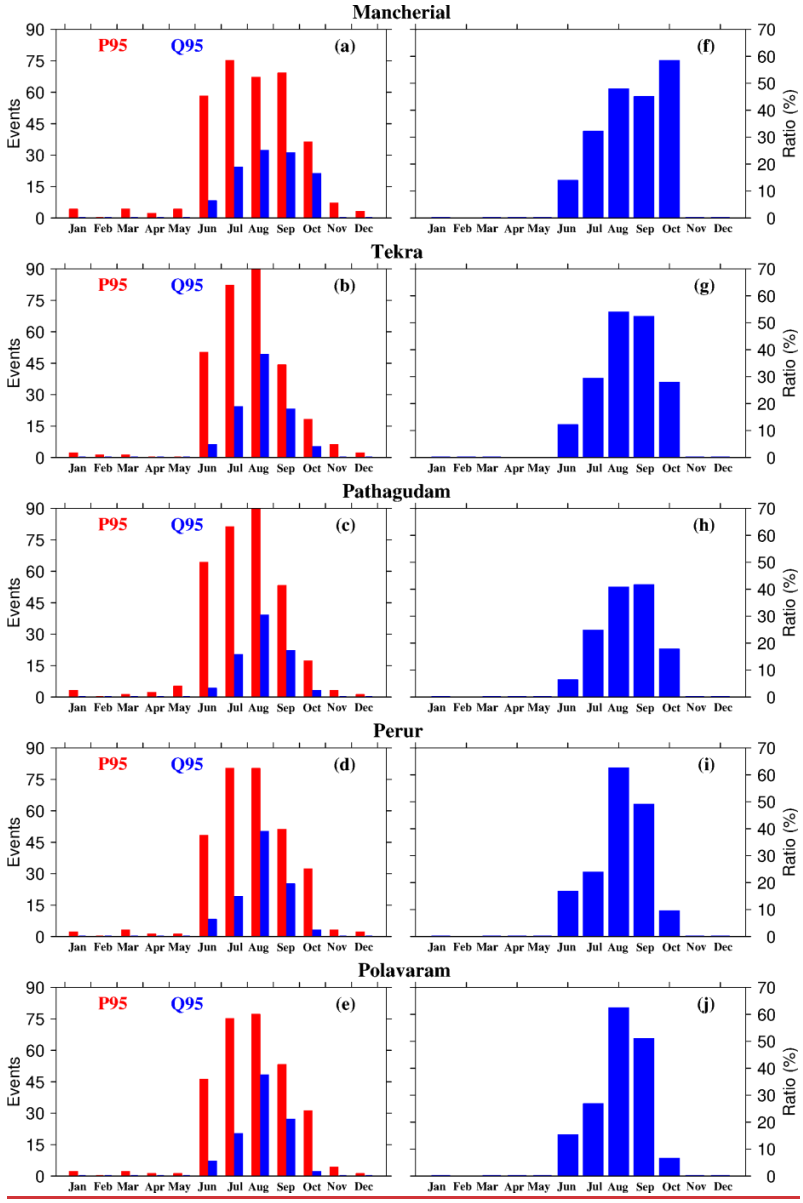


Figure S4. (a-e) Occurrence of high-intensity precipitation (P_{95}) and streamflow (Q_{95}) events (above 95th percentile) during 1967-2019 in each month at (a) ~~Polavaram, (b)~~

Formatted: Superscript

~~Perur, (c) Tekra, (d)~~ Mancherial, ~~and (e~~(b) Tekra, (c) Pathagudam, (d) Perur, and (e) Polavaram stations. (f-j) Ratio of the number of extreme streamflow and precipitation events in each month at ~~Polavaram, Perur, Tekra,~~ Mancherial, ~~and~~Tekra, Pathagudam, Perur, and Polavaram stations, respectively.

Formatted: Font: +Headings CS (Times New Roman), Bold

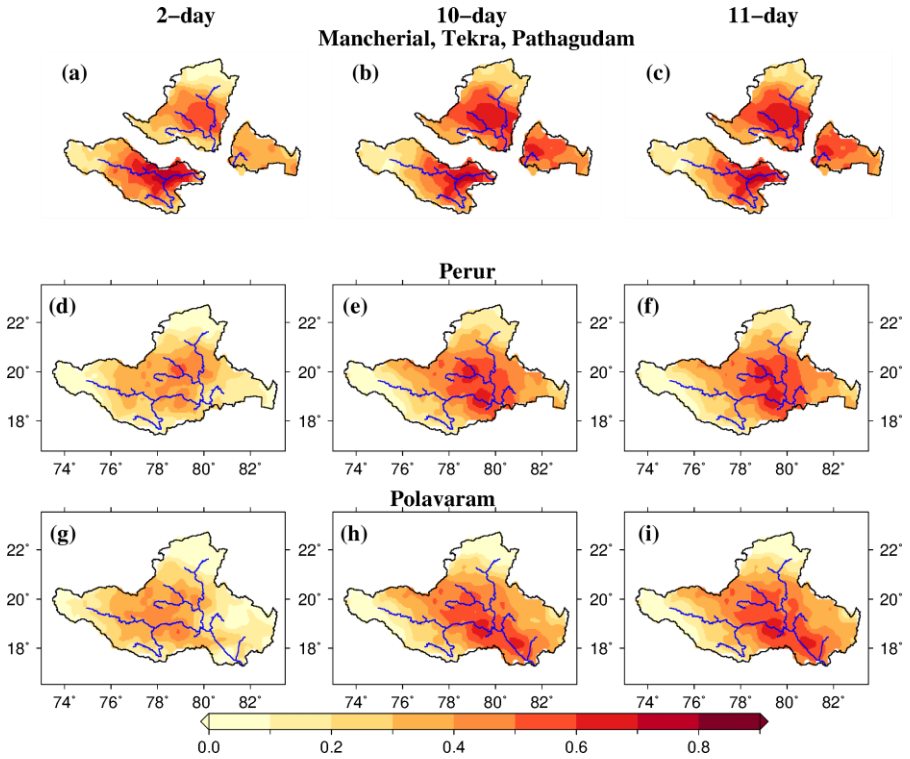


Figure ~~S4~~S5. Correlation between upstream accumulated precipitation and high-intensity streamflow at the basin downstream during 1967-2019. (a-c) Correlation between upstream precipitation and high-intensity streamflow at Mancherial (left), Tekra (middle), and Pathagudem (right) sub-basins using (a) 2 days, (b) 10 days, and (c) 11 days cumulative precipitation with 2 days lag period. (d-f) Similar to (a-c) but for the Perur sub-basin. (g-i) Similar to (a-c) but for Polavaram.

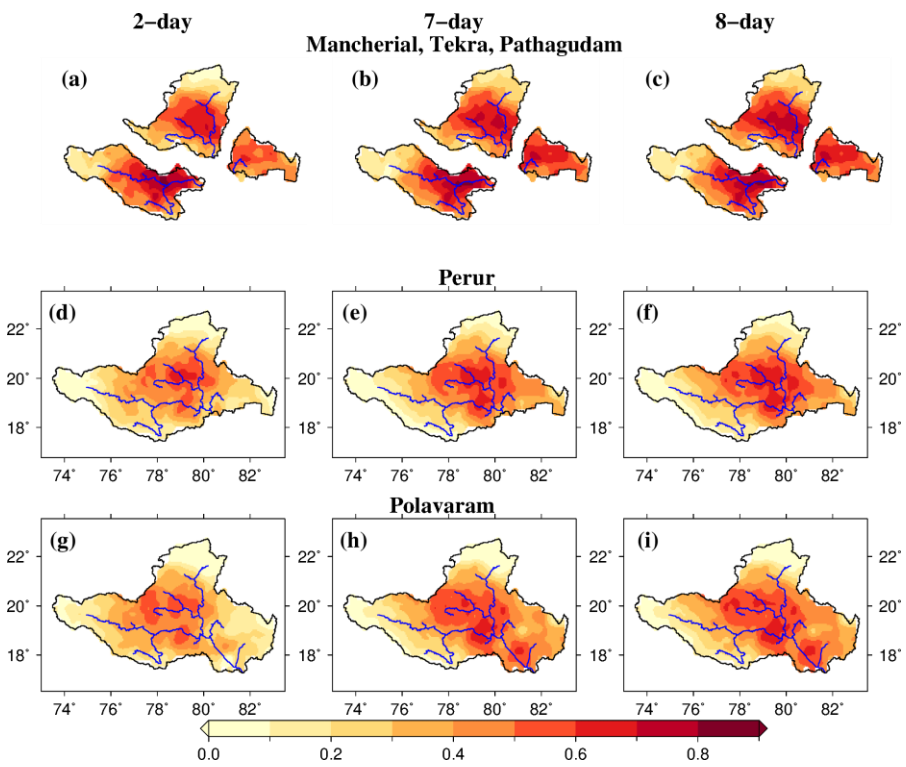


Figure ~~S5~~S6. Correlation between runoff and high-intensity streamflow at the basin downstream during 1967-2019. (a-c) Correlation between upstream runoff and high-

intensity streamflow at Mancherial (left), Tekra (middle), and Pathagudem (right) sub-basins using (a) 2 days, (b) 7 days, and (c) 8 days ~~cumulative~~mean runoff with 2 days lag period. (d-f) Similar to (a-c) but for the Perur sub-basin. (g-i) Similar to (a-c) but for Polavaram.

Table S1: Values of performance indices [NSE, Coefficient of determination (R^2), high flow bias (Bias_Q95), low flow bias (Bias_Q5) and bias of the mean (Bias_mean)] during the calibration of VIC simulated discharge (against the observed discharge data) for the period 1970-1979.

Calibration (1970-1979)					
Station	NSE	R^2	Bias_Q95 (%)	Bias_Q5 (%)	Bias_mean (%)
Mancherial	0.66	0.67	6.29	250.21	16.94
Tekra	0.8	0.86	39.57	-62.85	28

Pathagudam	0.6	0.61	18.45	-5.66	17.66
Perur	0.81	0.86	19.59	43.3	35.27
Polavaram	0.81	0.9	25.16	-41.43	37.44

1051

1052 Table S2: Values of performance indices [NSE, Coefficient of determination (R^2), and
1053 Bias] during the validation of VIC simulated discharge (against the observed discharge
1054 data) for the period 1980-2014 (except Mancherial station; 1980-1993 for Mancherial
1055 sub-basin).

Validation (1980-2014)					
Station	NSE	R^2	Bias_Q95 (%)	Bias_Q5 (%)	Bias_mean (%)
Mancherial*	0.52	0.59	88.52	190.3	79.26
Tekra	0.58	0.83	55.18	-74.17	53.76
Pathagudam	0.6	0.62	17.44	188.08	21.47
Perur	0.59	0.82	50.43	89.53	63.7
Polavaram	0.63	0.88	45.63	-55.78	56.37

1056 *validated for 1980-1993

1057 Table S3: Correlations between simulated streamflow peak and basin-averaged
1058 accumulated observed precipitation (prior to the flood peak) for different durations (days)
1059 and lags (days). The analysis is for high streamflow events at the Mancherial station for
1060 the period 1969-2019. Highlighted number is the best correlation value.

Lag / Duration .	0	1	2	3	4	5	6	7
1	-0.002	0.248	0.764	0.625	0.386	0.155	0.043	0.154
2	0.190	0.713	0.855	0.626	0.336	0.113	0.112	0.063
3	0.687	0.823	0.852	0.610	0.278	0.150	0.065	0.094
4	0.807	0.823	0.840	0.564	0.287	0.106	0.090	0.105
5	0.806	0.813	0.812	0.553	0.236	0.122	0.099	0.142
6	0.795	0.788	0.803	0.498	0.236	0.127	0.132	0.170
7	0.770	0.786	0.759	0.480	0.230	0.153	0.157	0.183
8	0.768	0.750	0.733	0.461	0.244	0.174	0.170	0.184
9	0.733	0.729	0.711	0.454	0.256	0.186	0.173	0.171
10	0.716	0.711	0.698	0.452	0.264	0.188	0.162	0.208
11	0.700	0.702	0.688	0.451	0.262	0.178	0.198	0.230
12	0.692	0.693	0.683	0.441	0.250	0.211	0.220	0.248
13	0.684	0.689	0.668	0.425	0.278	0.232	0.239	0.266
14	0.681	0.676	0.652	0.442	0.295	0.250	0.257	0.278
15	0.668	0.661	0.659	0.450	0.309	0.268	0.270	0.273
16	0.654	0.669	0.660	0.458	0.324	0.281	0.266	0.265
17	0.661	0.672	0.661	0.466	0.334	0.278	0.260	0.254
18	0.665	0.673	0.660	0.471	0.330	0.272	0.251	0.255
19	0.666	0.672	0.658	0.464	0.325	0.264	0.252	0.248
20	0.666	0.670	0.651	0.459	0.316	0.265	0.245	0.240

1061

1062 Table S4: Same as Table S3 but for the Tekra sub-basin.

Lag / Duration .	0	1	2	3	4	5	6	7

1	-0.029	0.238	0.576	0.510	0.178	0.164	0.243	0.252
2	0.152	0.572	0.674	0.473	0.207	0.223	0.290	0.326
3	0.541	0.688	0.649	0.475	0.255	0.291	0.359	0.425
4	0.674	0.662	0.651	0.491	0.319	0.354	0.449	0.467
5	0.648	0.665	0.659	0.521	0.376	0.442	0.483	0.505
6	0.651	0.670	0.681	0.547	0.456	0.476	0.518	0.491
7	0.656	0.693	0.699	0.589	0.487	0.512	0.506	0.483
8	0.680	0.714	0.722	0.607	0.522	0.504	0.499	0.492
9	0.704	0.738	0.725	0.634	0.515	0.501	0.507	0.492
10	0.733	0.739	0.743	0.628	0.513	0.509	0.506	0.458
11	0.735	0.754	0.738	0.620	0.522	0.509	0.475	0.442
12	0.750	0.747	0.728	0.622	0.526	0.484	0.461	0.438
13	0.743	0.738	0.724	0.630	0.504	0.472	0.459	0.422
14	0.733	0.733	0.726	0.614	0.493	0.472	0.444	0.427
15	0.728	0.733	0.711	0.605	0.492	0.459	0.450	0.424
16	0.728	0.719	0.704	0.605	0.481	0.465	0.446	0.418
17	0.713	0.712	0.701	0.595	0.486	0.460	0.439	0.392
18	0.706	0.708	0.691	0.598	0.482	0.454	0.414	0.393
19	0.703	0.697	0.693	0.593	0.475	0.429	0.414	0.411
20	0.693	0.699	0.686	0.585	0.450	0.429	0.429	0.396

Table S5: Same as Table S3 but for the Pathagudam sub-basin.

Lag / Duration .	0	1	2	3	4	5	6	7
1	-0.122	-0.198	0.354	0.485	0.477	0.242	0.152	0.182
2	-0.216	0.275	0.501	0.587	0.444	0.236	0.209	0.254

3	0.257	0.447	0.608	0.599	0.419	0.289	0.283	0.253
4	0.440	0.562	0.641	0.599	0.455	0.352	0.293	0.284
5	0.557	0.602	0.643	0.643	0.497	0.367	0.312	0.326
6	0.594	0.608	0.672	0.674	0.495	0.376	0.351	0.326
7	0.599	0.636	0.706	0.660	0.493	0.414	0.353	0.314
8	0.626	0.668	0.709	0.660	0.520	0.416	0.342	0.288
9	0.658	0.674	0.715	0.678	0.516	0.402	0.317	0.282
10	0.665	0.682	0.731	0.665	0.503	0.379	0.310	0.291
11	0.673	0.700	0.718	0.648	0.482	0.373	0.319	0.290
12	0.694	0.689	0.709	0.632	0.473	0.382	0.321	0.273
13	0.683	0.681	0.702	0.620	0.477	0.383	0.303	0.274
14	0.674	0.674	0.695	0.622	0.479	0.365	0.303	0.277
15	0.668	0.670	0.704	0.627	0.463	0.362	0.306	0.276
16	0.665	0.680	0.714	0.613	0.459	0.363	0.303	0.264
17	0.674	0.691	0.707	0.606	0.457	0.359	0.290	0.249
18	0.686	0.685	0.702	0.603	0.451	0.345	0.275	0.249
19	0.680	0.682	0.703	0.600	0.437	0.326	0.275	0.254
20	0.677	0.686	0.705	0.588	0.418	0.323	0.279	0.265

Table S6. Same as Table S3 but for Perur sub-basin.

Duration \ Lag	0	1	2	3	4	5	6	7
1	-0.054	0.178	0.558	0.544	0.326	0.250	0.207	0.135
2	0.090	0.509	0.651	0.509	0.335	0.263	0.209	0.206
3	0.471	0.637	0.627	0.517	0.346	0.281	0.261	0.292

4	0.617	0.619	0.631	0.523	0.373	0.322	0.330	0.389
5	0.601	0.622	0.636	0.541	0.410	0.377	0.411	0.438
6	0.604	0.626	0.650	0.563	0.456	0.443	0.458	0.433
7	0.609	0.643	0.675	0.591	0.512	0.488	0.454	0.403
8	0.626	0.671	0.699	0.630	0.553	0.486	0.425	0.398
9	0.655	0.699	0.722	0.659	0.547	0.458	0.420	0.393
10	0.685	0.721	0.738	0.651	0.518	0.453	0.415	0.375
11	0.710	**0.735**	0.729	0.624	0.510	0.448	0.398	0.365
12	0.725	0.726	0.705	0.614	0.507	0.431	0.389	0.358
13	0.716	0.704	0.693	0.611	0.490	0.422	0.382	0.343
14	0.695	0.693	0.690	0.595	0.480	0.415	0.368	0.342
15	0.684	0.691	0.678	0.585	0.473	0.402	0.367	0.341
16	0.683	0.680	0.670	0.579	0.460	0.400	0.364	0.339
17	0.671	0.673	0.665	0.570	0.457	0.396	0.362	0.325
18	0.665	0.668	0.659	0.566	0.450	0.393	0.348	0.330
19	0.660	0.664	0.659	0.557	0.446	0.379	0.352	0.349
20	0.656	0.665	0.651	0.550	0.431	0.382	0.369	0.351

Table S7: Same as Table S3 but for the Polavaram sub-basin.

Lag / Duration	0	1	2	3	4	5	6	7
1	0.084	0.152	0.347	0.613	0.556	0.382	0.182	0.036
2	0.138	0.317	0.573	0.647	0.533	0.344	0.130	0.190
3	0.312	0.551	0.641	0.648	0.511	0.305	0.243	0.263
4	0.544	0.626	0.654	0.637	0.503	0.389	0.307	0.319
5	0.618	0.642	0.649	0.633	0.569	0.426	0.354	0.376

Formatted Table

6	0.635	0.637	0.646	0.675	0.600	0.452	0.403	0.408
7	0.631	0.633	0.681	0.702	0.611	0.486	0.435	0.383
8	0.629	0.669	0.705	0.712	0.629	0.510	0.410	0.366
9	0.664	0.696	0.717	0.724	0.636	0.484	0.393	0.350
10	0.692	0.711	0.733	0.727	0.606	0.462	0.378	0.341
11	0.709	0.728	0.739	0.701	0.578	0.446	0.370	0.332
12	0.728	**0.736**	0.719	0.678	0.558	0.437	0.361	0.330
13	**0.736**	0.719	0.699	0.660	0.545	0.426	0.359	0.336
14	0.720	0.700	0.685	0.647	0.533	0.423	0.365	0.341
15	0.702	0.687	0.676	0.637	0.527	0.428	0.370	0.344
16	0.691	0.680	0.668	0.631	0.528	0.430	0.372	0.339
17	0.684	0.673	0.664	0.632	0.528	0.431	0.366	0.329
18	0.678	0.670	0.667	0.631	0.528	0.424	0.356	0.338
19	0.675	0.674	0.668	0.630	0.518	0.413	0.363	0.353
20	0.679	0.676	0.667	0.621	0.504	0.418	0.377	0.354

Table S8. Correlations between simulated streamflow peak and basin-averaged ~~accumulated~~mean simulated surface runoff (prior to the flood peak) for different durations (days) and lags (days). The analysis is for high streamflow events at the Mancherial station for the period 1969-2019. The highlighted number is the best correlation value.

Lag / Duration	0	1	2	3	4	5	6	7
1	0.100	0.368	0.850	0.743	0.485	0.226	0.060	0.232
2	0.340	0.831	0.955	0.750	0.453	0.174	0.177	0.107

3	0.825	0.937	0.960	0.745	0.391	0.239	0.107	0.142
4	0.929	0.943	0.955	0.713	0.421	0.174	0.136	0.169
5	0.935	0.940	0.943	0.719	0.359	0.189	0.155	0.205
6	0.931	0.929	0.943	0.677	0.354	0.201	0.188	0.243
7	0.921	0.934	0.923	0.659	0.351	0.225	0.224	0.264
8	0.925	0.917	0.905	0.647	0.359	0.254	0.245	0.266
9	0.909	0.903	0.896	0.630	0.371	0.272	0.249	0.247
10	0.896	0.895	0.884	0.623	0.383	0.275	0.233	0.288
11	0.889	0.887	0.875	0.620	0.380	0.260	0.275	0.300
12	0.882	0.880	0.871	0.610	0.365	0.296	0.290	0.319
13	0.875	0.876	0.860	0.593	0.391	0.310	0.309	0.334
14	0.872	0.866	0.849	0.599	0.397	0.329	0.325	0.343
15	0.863	0.857	0.847	0.591	0.412	0.344	0.335	0.335
16	0.853	0.857	0.836	0.596	0.422	0.354	0.329	0.326
17	0.852	0.849	0.834	0.598	0.429	0.348	0.322	0.315
18	0.845	0.848	0.829	0.597	0.421	0.342	0.312	0.315
19	0.844	0.843	0.823	0.588	0.416	0.332	0.313	0.310
20	0.840	0.837	0.815	0.583	0.406	0.333	0.308	0.303

1075

1076 Table S9. Same as Table S8 but for the Tekra sub-basin.

Lag / Duration .	0	1	2	3	4	5	6	7
1	0.014	0.391	0.774	0.748	0.343	0.224	0.342	0.301
2	0.310	0.775	0.910	0.758	0.339	0.311	0.369	0.395
3	0.762	0.913	0.924	0.747	0.394	0.381	0.447	0.492
4	0.909	0.922	0.928	0.758	0.451	0.449	0.528	0.533

5	0.916	0.929	0.933	0.762	0.505	0.530	0.560	0.561
6	0.922	0.933	0.933	0.767	0.574	0.562	0.581	0.553
7	0.924	0.936	0.937	0.775	0.599	0.588	0.575	0.550
8	0.927	0.943	0.931	0.777	0.621	0.583	0.572	0.560
9	0.937	0.942	0.920	0.784	0.616	0.584	0.580	0.562
10	0.940	0.930	0.917	0.776	0.615	0.591	0.579	0.535
11	0.929	0.925	0.910	0.771	0.624	0.590	0.554	0.515
12	0.924	0.918	0.905	0.769	0.624	0.569	0.536	0.506
13	0.917	0.913	0.897	0.769	0.606	0.554	0.529	0.489
14	0.911	0.905	0.892	0.755	0.590	0.548	0.514	0.497
15	0.902	0.899	0.879	0.741	0.584	0.535	0.522	0.493
16	0.896	0.887	0.867	0.732	0.570	0.542	0.516	0.482
17	0.884	0.875	0.857	0.720	0.576	0.535	0.505	0.466
18	0.873	0.864	0.844	0.718	0.568	0.524	0.490	0.482
19	0.862	0.851	0.841	0.708	0.556	0.509	0.504	0.504
20	0.849	0.848	0.831	0.696	0.541	0.522	0.522	0.478

1077

1078 Table S10. Same as Table S8 but for the Pathagudam sub-basin.

Lag / Duration .	0	1	2	3	4	5	6	7
1	-0.059	-0.088	0.528	0.697	0.584	0.289	0.187	0.185
2	-0.102	0.480	0.765	0.758	0.547	0.289	0.229	0.302
3	0.480	0.735	0.851	0.764	0.523	0.335	0.333	0.322
4	0.736	0.834	0.873	0.768	0.549	0.416	0.362	0.365
5	0.836	0.862	0.872	0.799	0.596	0.444	0.391	0.412
6	0.857	0.864	0.887	0.820	0.602	0.459	0.436	0.415

7	0.858	0.877	0.910	0.804	0.602	0.502	0.442	0.404
8	0.870	0.896	0.907	0.800	0.632	0.510	0.433	0.375
9	0.888	0.895	0.905	0.815	0.635	0.501	0.407	0.359
10	0.889	0.893	0.916	0.810	0.627	0.478	0.392	0.364
11	0.887	0.905	0.909	0.802	0.608	0.465	0.396	0.360
12	0.901	0.898	0.907	0.787	0.594	0.468	0.394	0.345
13	0.895	0.897	0.900	0.773	0.592	0.464	0.380	0.351
14	0.894	0.891	0.891	0.768	0.588	0.450	0.384	0.351
15	0.888	0.882	0.892	0.765	0.575	0.450	0.384	0.349
16	0.881	0.884	0.894	0.752	0.572	0.448	0.380	0.334
17	0.882	0.888	0.888	0.747	0.566	0.442	0.364	0.323
18	0.885	0.883	0.882	0.737	0.556	0.424	0.353	0.330
19	0.880	0.878	0.873	0.728	0.539	0.409	0.359	0.337
20	0.875	0.871	0.868	0.713	0.523	0.412	0.364	0.346

Table S11. Same as Table S8 but for the Perur sub-basin.

Lag / Duration	0	1	2	3	4	5	6	7
1	-0.005	0.338	0.742	0.776	0.475	0.323	0.290	0.221
2	0.249	0.724	0.891	0.764	0.470	0.357	0.318	0.290
3	0.714	0.888	0.896	0.766	0.487	0.401	0.368	0.373
4	0.884	0.892	0.900	0.774	0.535	0.440	0.427	0.462
5	0.884	0.896	0.906	0.795	0.563	0.482	0.495	0.508
6	0.888	0.900	0.920	0.791	0.592	0.531	0.537	0.506
7	0.891	0.916	0.930	0.787	0.626	0.572	0.534	0.483
8	0.907	**0.930**	0.924	0.797	0.659	0.571	0.513	0.479

9	0.921	**0.930**	0.917	0.809	0.651	0.551	0.508	0.473
10	0.923	0.923	0.916	0.797	0.629	0.545	0.500	0.452
11	0.917	0.919	0.903	0.778	0.621	0.537	0.480	0.438
12	0.914	0.906	0.889	0.765	0.613	0.517	0.467	0.431
13	0.902	0.894	0.876	0.756	0.592	0.503	0.459	0.416
14	0.889	0.880	0.867	0.736	0.577	0.496	0.446	0.417
15	0.876	0.873	0.853	0.721	0.569	0.483	0.446	0.416
16	0.869	0.860	0.839	0.714	0.556	0.481	0.443	0.408
17	0.855	0.847	0.833	0.703	0.551	0.477	0.435	0.397
18	0.843	0.841	0.824	0.694	0.543	0.468	0.424	0.415
19	0.837	0.833	0.819	0.683	0.532	0.457	0.440	0.439
20	0.829	0.829	0.808	0.669	0.521	0.472	0.461	0.433

Table S12. Same as Table S8 but for the Polavaram sub-basin.

Lag / Duration	0	1	2	3	4	5	6	7
1	0.132	0.310	0.532	0.857	0.692	0.443	0.279	0.149
2	0.274	0.523	0.845	0.865	0.658	0.441	0.258	0.281
3	0.531	0.833	0.895	0.853	0.657	0.439	0.360	0.343
4	0.829	0.884	0.888	0.855	0.681	0.513	0.403	0.397
5	0.877	0.880	0.891	0.869	0.736	0.524	0.446	0.451
6	0.875	0.882	0.904	0.890	0.738	0.546	0.487	0.480
7	0.877	0.894	0.923	0.890	0.738	0.573	0.515	0.459
8	0.891	0.915	0.920	0.882	0.740	0.593	0.495	0.447
9	0.910	0.917	0.913	0.876	0.737	0.571	0.482	0.438
10	0.914	0.913	0.910	0.865	0.713	0.554	0.473	0.426

11	0.912	0.912	0.902	0.846	0.693	0.544	0.461	0.416
12	0.913	0.906	0.888	0.830	0.677	0.532	0.450	0.411
13	0.907	0.893	0.874	0.815	0.660	0.520	0.445	0.416
14	0.895	0.880	0.862	0.798	0.646	0.513	0.450	0.419
15	0.882	0.869	0.850	0.785	0.636	0.516	0.452	0.422
16	0.872	0.857	0.840	0.776	0.635	0.516	0.454	0.416
17	0.861	0.849	0.832	0.773	0.631	0.516	0.446	0.407
18	0.853	0.842	0.829	0.766	0.629	0.507	0.437	0.425
19	0.846	0.839	0.824	0.763	0.617	0.497	0.453	0.447
20	0.845	0.835	0.820	0.751	0.605	0.511	0.473	0.442

1083